A Novel Event-Triggered Secondary Control Strategy for Distributed Generalized Droop Control in Microgrid Considering Time Delay

Jiancheng Zhang, Bo Sun, *Member, IEEE*, and Daduan Zhao, *Member, IEEE*

***Abstract*—With the wide use of new energy and power electronic devices, the problem of low inertia of microgrid (MG) is becoming more and more prominent. In order to solve the problem, this article proposes an event-triggered secondary control strategy for distributed generalized droop control (GDC) considering time delay. First, a distributed event-triggered active power and frequency controllers are established based on GDC, and a distributed voltage controller is designed based on droop control. Second, due to the different frequency parameters of each distributed generator (DG), the tracking controller of frequency and frequency reference model is established by using heterogeneous multiagent theory. Third, the event-triggered function of communication between DGs is constructed, and the stability of the proposed controller is proved. The complicated Lyapunov equation is avoided in the proof process. Finally, the effectiveness of the controller is verified by simulation. The simulation results show that the controller effectively realizes the secondary adjustment of frequency and voltage, reduces the number of communications, and increases the inertia of MG.**

***Index Terms*—Distributed generator, event-triggered control, generalized droop control, microgrid, time delay.**

I. Introduction

MICROGRID (MG) is a small distributed system, which usually consists of distributed generators (DGs) and load and energy storage equipment [1], [2]. Due to its flexibility, MG has been widely used in many fields, such as ships, smart buildings, islands, and space stations. With the development of information technology and power electronics in recent years, the combined utilization of MG and clean energy has become more popular. In order to ensure the stable and efficient operation of MG, the effective control strategy is needed.

MG control strategy usually adopts a hierarchical control mode [3]. The droop control usually acts as the primary control in the MG. However, traditional droop control is susceptible to line impedance and load fluctuation. The droop control belongs to proportional control, which will lead to steady-state errors in the voltage and frequency of DG. In addition, when the traditional droop control is adopted, due to the influence of impedance mismatch of the DG feeders and the different ratings of the DG units, the poor active and reactive power sharing problems are inevitable [4]. Therefore, it is necessary to introduce secondary control into MG to solve the shortage of primary control. When considering the operation cost and economic dispatch of MG, tertiary control should be introduced. The research object of this article is secondary control.

In order to make up the deficiency of traditional droop control and improve the reliability and flexibility of MG, the secondary control based on multiagent theory has been widely studied [5], [6], [7]. For example, Malik et al. [8] proposed a generalized droop control method. This method is able to achieve power sharing, and improve the frequency response characteristics of MG. Riverso et al. [9] proposed a distributed hierarchical control strategy. This strategy is used to stabilize the frequency and voltage with desired reactive power sharing. In addition to the above methods, many other different secondary controllers for MG are also considered, such as, fault tolerant control [10], robust control [11], [12], and H∞ consensus-based control [13]. The control techniques used in the above literatures adopt continuous communication. These methods assume that multiagent systems have unlimited memory and computing resources. But these hardware resources are limited in actual use [14]. Therefore, it is necessary to save communication resources.

In order to reduce the number of communications and save communication resources, the MG consistency control using continuous event-triggered communication is presented [15], [16], [17]. For example, Choi et al. [18] proposed an event-triggered frequency and voltage regulation strategy of islanded MG. This control method uses event-triggered communication to reduce the communication burden between DG controllers. Chen et al. [19] proposed a hierarchical event-triggered control strategy. This control method also realizes the secondary regulation of MG. Guo et al. [20] proposed a distributed voltage restoration and current sharing control without continuous communication. The above three control methods both adopt the continuous event-triggered control strategy. When using the continuous event-triggered control strategy, this control strategy needs to prove that the system does not have Zeno behavior. In [21] and [22], a periodic event-triggered control method was proposed. This method ensures that there is at least one time

Manuscript received 6 September 2022; revised 19 December 2022; accepted 17 January 2023. Date of publication 31 January 2023; date of current version 10 March 2023. This work was supported in part by the National Natural Science Foundation of China under Grants 61821004, 62192753, and 62133008 and in part by the Natural Science Foundation of Shandong province under Grant ZR2019ZD09. Recommended for publication by Associate Editor K. Gunawardane. *(Corresponding author: Bo Sun.)*

The authors are with the School of Control Science and Engineering, Shandong University, Jinan 250061, China (e-mail: zhangjiancheng@sdu.edu.cn; sunbo@sdu.edu.cn; zhaodaduan@mail.sdu.edu.cn).

Color versions of one or more figures in this article are available at https://doi.org/10.1109/TPEL.2023.3241063.

Digital Object Identifier 10.1109/TPEL.2023.3241063

interval between adjacent trigger events. However, this method may produce redundant packets, and some critical data may be discarded. Typical event-triggered control methods for MG can be found in [15], [16], [17], [18], [19], [20], [21], [22], [23] and their references. However, for nonlinear multiagent systems with directed graph, the event-triggered consensus control considering time delay is rarely studied.

The MG secondary control methods mentioned in references [5], [6], [7], [8], [9], [10], [11], [12], [13], [14], [15], [16], [17], [18], [19], [20], [21], [22], [23] are based on the traditional droop control as the primary control. Due to the use of power electronic devices in MG and the characteristics of DG, MG is a small system with low inertia. Because the traditional droop control method does not have the ability to adjust the inertia of MG. Therefore, many scholars use virtual synchronous generator (VSG) technology to enhance the inertia of MG [24]. VSG can provide damping characteristics and virtual inertia for inverter. This control method simulates the motion of traditional synchronous generator rotor, but it only realizes the primary control of frequency [25], [26], [27]. At present, many researchers use the virtual governor method to realize the secondary control of MG based on VSG technology [28]. In [29], an alternating direction multipliers method for VSG is proposed to provide additional inertia and damping moments. Shi et al. [30] proposed a frequency secondary controller based on distributed VSG, which can restrain frequency oscillation. But these methods can not eliminate the frequency deviation. In addition, in these literatures, the inertia parameters and damping parameters of all controllers are set to the same values, respectively, but in fact they may be different. If the inertia parameters and damping parameters are set to different values, respectively, the parameter design of secondary control based on VSG will be very complex due to the influence of line impedance and load.

Although the above distributed control method based on VSG can improve the inertia and damping characteristics of MG, the frequency of MG will still experience low-frequency oscillation when the load fluctuates or the structure changes in MG [31]. In [32], the authors proposed a generalized droop control (GDC) method, which can improve the oscillation of the frequency of MG. However, the author did not further design the secondary control of MG to eliminate the frequency deviation. Inspired by this, if GDC method is introduced into distributed frequency secondary control, the inertia and damping characteristics of MG will be improved. As far as the author knows, the secondary control for distributed GDC in MG has not been studied yet.

In this article, based on the problems and shortcomings of the research in the above literatures, a distributed GDC event-triggered secondary control method considering time delay is proposed. First, using feedback linearization method, a distributed event-triggered voltage controller with directed graph for MG considering time delay is designed based on droop control. Considering the same factors, an active power and frequency controllers are established based on GDC. Second, because the virtual inertia and damping of each DG are different, the design method of heterogeneous multiagent theory is used in the design of frequency controller. The reference model of the frequency controller is established, and the consistency of multiagent is used to make the frequency controllers converge with the reference model. Third, the event-triggered communication function of voltage controller, active power controller and frequency controller are established, so that the controller can communicate once when the trigger conditions are met. Finally, the stability of the controller is proved by the Newton–Leibnitz formula, and the effectiveness of the controller is verified by simulation.

The innovations of this article can be summarized as follows.

1) Different from [5], [6], [7], [8], [9], [10], [11], [12], [13], [14], [15], [16], [17], [18], [19], [20], [21], [22], [23], this article presents a distributed event-triggered frequency secondary controller and active power controller based on GDC, and the distributed event-triggered voltage secondary controller is designed by using the nonlinear multiagent system theory, considering directed graph and time delay. The proposed controller effectively realizes the secondary regulation of frequency and voltage of MG. Using event-triggered communication effectively reduces the number of communications.
2) Different from the existing control methods VSG and GDC [28], [29], [30], [32], the distributed GDC frequency secondary controller is constructed by using the heterogeneous multiagent theory, which avoids the complex parameter design and makes the control of MG more flexible. This method makes MG have better inertia and damping characteristics.
3) Different from the existing methods of proving the stability of distributed event-triggered controllers based on multiagent theory, this article uses Newton–Leibniz formula to strictly prove the stability of the designed controller. This avoids constructing complex Lyapunov equations for multiagent systems with directed graph considering time delay.

The rest of this article is arranged as follows. The Section II introduces the hierarchical control structure of MG and the mathematical model of each controller. In Section III, the stability of the proposed controller is proved by using related theorems. In Section IV, a simulation example is used to verify the effectiveness of the controller. Section V is the conclusion of this article.

II. Distributed Control Framework

The traditional droop control usually acts as the primary control in MG. Fig. 1 shows the internal structure of DG. Because the *LC* filter is used in the circuit, the circuit is inductive. So, the equation of the droop control can be written as

$$\begin{cases} \omega_i = \omega_{ni} - m_i \left(P_i - P_{seti}\right) \\ U_i = U_{ni} - n_i \left(Q_i - Q_{seti}\right) \end{cases} \tag{1}$$

where m_i and n_i are the droop coefficients. P_{seti} and Q_{seti} are the active power command and reactive power command, respectively. ω_i is the reference frequency output by the droop controller. U_i is the reference voltage output by the droop controller. ω_{ni} and U_{ni} are nominal frequency and voltage. Q_i and P_i are the measured reactive power and active power,

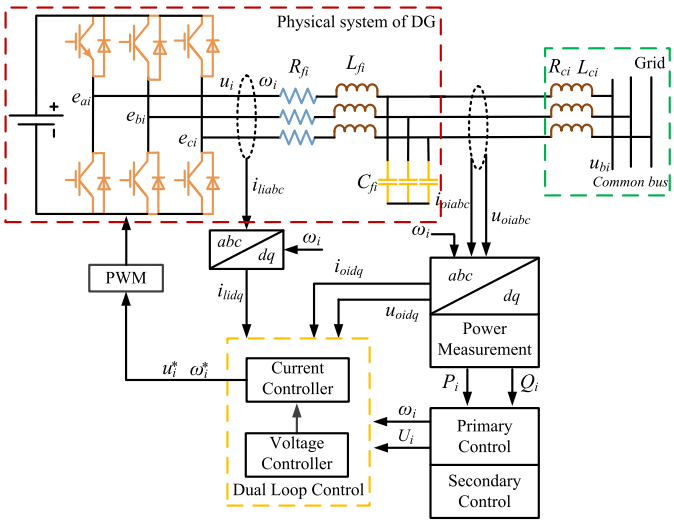

Fig. 1. Internal structure diagram of DG.

respectively. The first item of the above equation can be written as

$$\frac{\omega_i - \omega_{ni}}{P_i - P_{seti}} = -m_i. \tag{2}$$

Since the droop control does not have the ability to adjust the inertia of MG, this article uses the GDC as the primary control of MG. Next, the primary controller and secondary controller will be introduced in detail.

A. Primary Controller

The principle that VSG provides virtual inertia is to imitate the rotor of synchronous motor. The mathematical expression of its physical model can be written as [32]

$$J_i\omega_{ni}\frac{d\omega_i}{dt} = P_{seti} - P_i - D_{pi}(\omega_i - \omega_{ni}) \tag{3}$$

where D_{pi} is the damping factor, P_{seti} is the active power command, and J_i is the rotor inertia.

Although VSG-based controller can improve the inertia of the inverter, the frequency and power curves of MG will still fluctuate violently when the topology structure or load of MG changes [31], [32]. In order to further improve the inertia and damping characteristics of the inverter, we need to further improve the controller. Equation (3) can be written as

$$\begin{aligned}\frac{\omega_i - \omega_{ni}}{P_i - P_{seti}} &= -\frac{1}{J_i\omega_{ni}s + D_{pi}} \\ &= -\frac{1}{D_{pi}} \cdot \frac{1}{\frac{J_i\omega_{ni}}{D_{pi}}s + 1}.\end{aligned} \tag{4}$$

Comparing (2) and (4), we find that VSG control is equivalent to the droop control when the inertia is not considered, i.e., $J_i = 0$. Therefore, the droop control is a VSG control in a special case. Inspired by this, we can further extend (4) as (5). In (5), the $-\frac{K_i}{T_{1i}s+1}$ term is similar to the VSG control method to increase the inertia and damping characteristics of the system. $\tau_{1i}s + 1$ item is to increase the phase margin [32]. $T_{2i}s + 1$ item is to reduce the high-frequency gain to ensure a smooth angular frequency change when the load power change

$$\begin{aligned}\frac{\omega_i - \omega_{ni}}{P_i - P_{seti}} &= -\frac{K_i(\tau_{1i}s + 1)}{(T_{1i}s + 1)(T_{2i}s + 1)} \\ &= -\frac{d_is + e_i}{a_is^2 + b_is + c_i}.\end{aligned} \tag{5}$$

The above equation can be extended to a more general form. The specific design process of (5) can be found in [32]. In [32], the authors only considered the response characteristics of the frequency and power of DG, and did not make further secondary adjustment to the frequency and power. This does not solve the problem of frequency deviation mentioned above. Different from [32], we use (5) as the primary controller of DG to improve the inertia and damping characteristics of the inverter. On this basis, a secondary controller is designed to adjust the voltage and frequency of MG. In Section C, we will describe the contents of this part in detail.

B. Mathematical Preliminaries

It is necessary to introduce the basic knowledge of multiagent theory before introducing the controller based on multiagent theory. The communication network of multiagent system can be described by graph theory. The following controller introduction and controller stability proof will use the relevant knowledge of graph theory.

According to graph theory, the communication network of a multiagent system can usually be expressed as $G = \{V, \Xi, A\}$, where $V = \{v_1, v_2, \ldots, v_N\}$ is the node set. (v_j, v_i) means that node i can receive information from node j. $A = [a_{ij}] \in R^{n\times n}$ is the weighted adjacency matrix. a_{ij} is the weight of edge (v_j, v_i). If $(v_j, v_i) \in \Xi$, $a_{ij} > 0$, otherwise $a_{ij} = 0$. Node i is the neighbor of node j if $(v_j, v_i) \in \Xi$, and the set of neighbors of node j is denoted as $N_j = \{i \in V | (v_i, v_j) \in \Xi\}$. The in-degree matrix $D^{in} = \text{diag}\{d_i^{in}\}$ is a diagonal matrix with $d_i^{in} = \sum_{j\in N_i} a_{ij}$. L is a Laplacian matrix. There is $L = D^{in} - A$. $B = \text{diag}\{b_1, b_2, \ldots, b_N\}$ is the leader adjacency matrix. $\|.\|$ denotes the induced 2-norm for matrix or the Euclidean norm for vector.

Different from the undirected graph multiagent system studied by most scholars, the multiagent system studied in this article is directed graph system. To enable information to be passed from the root node to each node, we introduce the following two assumptions.

Assumption 1: The directed graph G has a spanning tree whose root node is at agent 0, i.e., from the root node agent 0, all the other nodes can be reached along the edge directions in graph G. The communication weight $a_{ij} \geq 1$ and the element $b_i \geq 1$ of the leader adjacency matrix B.

Assumption 2: In the directed graph G, the information is transmitted from node i to j in one direction, and the node number satisfies $i > j$ or $i < j$ $\forall i, j = 1, \ldots, N$.

In proving the stability of the proposed controller, we will use some properties of the eigenvalues of matrices in graph theory.

So we will introduce three lemmas about the eigenvalues of matrices.

Lemma 1 ([33]): Under Assumption 1, the Laplacian matrix L has an eigenvalue 0, and all eigenvalues of L satisfy the following relation: $0 = \lambda_1(L) < \mathrm{Re}(\lambda_i(L)) \leq \cdots \leq \mathrm{Re}(\lambda_N(L))$, where $\mathrm{Re}(\lambda_i(L))$ denotes the real part of the characteristic root λ_i.

Lemma 2 ([34]): Under Assumption 1, the matrix $L+B$ is positive stable.

Lemma 3: There is $\mathrm{Re}(\lambda_N(T+N)) < 0$, i.e., the maximum value of the real part of the eigenvalue of matrix $T+N$ is less than 0, where the matrix $N = \begin{pmatrix} 0 & 0 \\ -(L+B) & -(L+B) \end{pmatrix}$ and $T = \begin{pmatrix} 0 & I_N \\ 0 & 0 \end{pmatrix}$.

Proof: We set that λ is the eigenvalue of $T+N$ and ς is the eigenvalue of $L+B$. Then, there is

$$\begin{aligned} &\begin{vmatrix} \mathbf{0} - \lambda I_N & I_N \\ -(L+B) & -(L+B) - \lambda I_N \end{vmatrix} \\ &= \det\left(\lambda^2 I_N + \lambda(L+B) + (L+B)\right) \\ &= 0. \end{aligned} \tag{6}$$

From (6), we can get

$$\prod_{1\leq i\leq N}\left(\lambda^2 + \lambda\varsigma_i + \varsigma_i\right) = 0. \tag{7}$$

By solving the above equation, we can get

$$\lambda_{i1} = \frac{-\varsigma_i + \sqrt{\varsigma_i^2 - 4\varsigma_i}}{2}, \lambda_{i2} = \frac{-\varsigma_i - \sqrt{\varsigma_i^2 - 4\varsigma_i}}{2}. \tag{8}$$

Let

$$\sqrt{\varsigma_i^2 - 4\varsigma_i} = d + iq \tag{9}$$

where $i = \sqrt{-1}$, d and q are real numbers. $\mathrm{Re}(\varsigma_i)$ and $\mathrm{Im}(\varsigma_i)$ are the real and imaginary parts of eigenvalue ς_i, respectively, i.e.,

$$\varsigma_i = \mathrm{Re}(\varsigma_i) + i\mathrm{Im}(\varsigma_i). \tag{10}$$

Then, there are

$$\begin{cases} \lambda_{i1} = \frac{(-\mathrm{Re}(\varsigma_i)+d)+\mathrm{i}(-\mathrm{Im}(\varsigma_i)+q)}{2} \\ \lambda_{i2} = \frac{(-\mathrm{Re}(\varsigma_i)-d)+\mathrm{i}(-\mathrm{Im}(\varsigma_i)-q)}{2}. \end{cases} \tag{11}$$

Now we want to prove that $\mathrm{Max}(\mathrm{Re}(\lambda_{i1}), \mathrm{Re}(\lambda_{i2})) < 0$ holds, i.e., $-\mathrm{Re}(\varsigma_i) + d < 0$ and $-\mathrm{Re}(\varsigma_i) - d < 0$. It is equivalent to $\mathrm{Re}(\varsigma_i)^2 > d^2$. Square both sides of (9) and substitute (10) into (9). Because the real part and imaginary part on both sides of (9) are equal, respectively, we can get

$$\mathrm{Re}(\varsigma_i)\mathrm{Im}(\varsigma_i) - 2\mathrm{Im}(\varsigma_i) = dq \tag{12}$$

$$\mathrm{Re}(\varsigma_i)^2 - 4\mathrm{Re}(\varsigma_i) - \mathrm{Im}(\varsigma_i)^2 = d^2 - q^2. \tag{13}$$

Substituting (12) into (13) yields

$$\begin{aligned} &\mathrm{Re}\,(\varsigma_i)^2 - d^2 \\ &= \mathrm{Im}\,(\varsigma_i)^2 + 4\,\mathrm{Re}\,(\varsigma_i) - q^2 \\ &= \frac{1}{d^2}\Big(\mathrm{Im}\,(\varsigma_i)^2 d^2 + 4\,\mathrm{Re}\,(\varsigma_i) d^2 \\ &\quad - \mathrm{Re}\,(\varsigma_i)^2 \mathrm{Im}\,(\varsigma_i)^2 - 4\,\mathrm{Im}\,(\varsigma_i)^2 + 4\,\mathrm{Re}\,(\varsigma_i)\,\mathrm{Im}\,(\varsigma_i)^2\Big) \\ &= \frac{\mathrm{Im}\,(\varsigma_i)^2}{d^2}\left(d^2 - \mathrm{Re}\,(\varsigma_i)^2\right) \\ &\quad + \frac{1}{d^2}\left(4\,\mathrm{Re}\,(\varsigma_i) d^2 + 4\,\mathrm{Re}\,(\varsigma_i)\,\mathrm{Im}\,(\varsigma_i)^2 - 4\,\mathrm{Im}\,(\varsigma_i)^2\right). \end{aligned} \tag{14}$$

Then, there is

$$\begin{aligned} &\left(\mathrm{Re}\,(\varsigma_i)^2 - d^2\right)\left(1 + \frac{\mathrm{Im}\,(\varsigma_i)^2}{d^2}\right) \\ &= \frac{4}{d^2}\left(\mathrm{Re}\,(\varsigma_i) d^2 + \mathrm{Re}\,(\varsigma_i)\,\mathrm{Im}\,(\varsigma_i)^2 - \mathrm{Im}\,(\varsigma_i)^2\right). \end{aligned} \tag{15}$$

■

Therefore, the proof of Lemma 3 is equivalent to the proof of the following inequality.

$$\mathrm{Re}(\varsigma_i)d^2 + \mathrm{Re}(\varsigma_i)\mathrm{Im}(\varsigma_i)^2 - \mathrm{Im}(\varsigma_i)^2 > 0. \tag{16}$$

We set $L+B$ as shown in the following (17)–(18) shown at the bottom of the next page.

According to Assumption 2, the information is transmitted from node i to j in one direction. We assume without loss of generality that $i < j$. Based on the properties of graph theory, we can conclude that (17) a lower triangular matrix. The eigenvalue ς of $L+B$ satisfies (18).

Then, we can get

$$\varsigma_i = \sum_{1\leq j\leq N}(a_{ij}) + b_i, i = 1, \ldots, N. \tag{19}$$

Because $a_{ij} \geq 1$ and $b_i \geq 1$, we have $\mathrm{Re}(\varsigma_i) \geq 1$. Then, (16) holds.

C. Secondary Frequency Controller

The schematic diagram of the proposed secondary controller is shown in Fig. 2. It includes frequency control, voltage control, and active power control. When the frequency of MG is adjusted using VSG control method, we usually use a virtual governor to adjust the frequency. Inspired by this, this article introduces the distributed secondary controller into GDC by using the virtual governor. Its theoretical equation can be expressed as

$$\omega_{ni} - \omega_i = \frac{1}{k_\omega} P_{\omega i} \tag{20}$$

where k_ω is the frequency regulation factor. To realize secondary frequency regulation, $P_{\omega i}$ is the power compensation provided by the governor. The derivative of both sides of (20) can be obtained as following:

$$\dot{\omega}_{ni} = \dot{\omega}_i + \frac{1}{k_\omega}\dot{P}_{\omega i}. \tag{21}$$

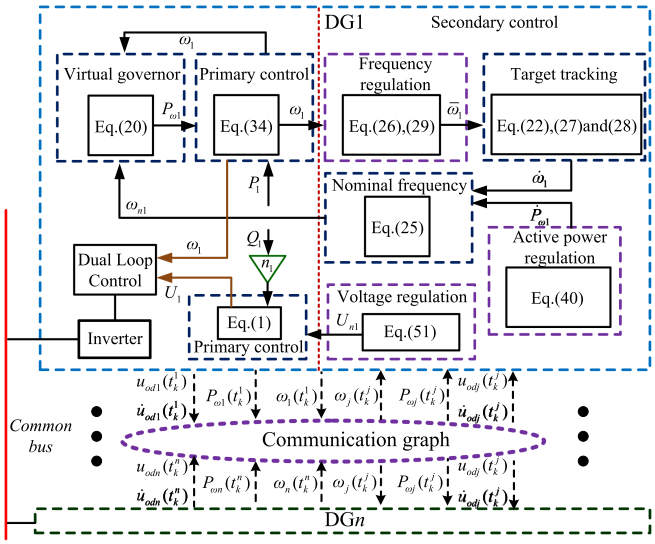

Fig. 2. Proposed secondary control schematic diagram.

According to (5), the expression of frequency controller can be designed as given in the following:

$$\dot{\omega}_i = f_i(\omega_i) + u_{\omega i} \tag{22}$$

$$f(\omega_i) = -\frac{1}{b_i}[(a_i s^2 + c_i)\omega_i - c_i\omega_{ni} - (d_i s + e_i)P_i + P_{seti}e_i] \tag{23}$$

where $u_{\omega i}$ is the control input. Comparing the first equation in (1) with (20), we can find that the two equations are similar in form. The secondary controller designed based on droop control achieves active power sharing by obtaining the consistency of $m_i(P_i - P_{seti})$. Inspired by this, we can indirectly realize active power sharing by realizing the consistency of active power compensation $P_{\omega i}$ (to simplification, the coefficient k_ω for all controllers is chosen to be the same value. Otherwise, $\frac{1}{k_{\omega i}}P_{\omega i} = \frac{1}{k_{\omega j}}P_{\omega j}$ is used to realize active power sharing). The expression of active power controller can be designed as

$$\dot{P}_{\omega i} = u_{pi} \tag{24}$$

Equation (21) can be rewritten as (25). Using (25), we can get the nominal frequency ω_{ni}

$$\omega_{ni} = \int \left(\dot{\omega}_i + \frac{1}{k_\omega}\dot{P}_{\omega i}\right)dt. \tag{25}$$

Due to the different inertia and damping parameters of each DG, a heterogeneous multiagent system is formed, so it is necessary to use the heterogeneous multiagent theory to design the frequency controller [35]. For the problem of heterogeneous multiagent convergence, we first need to establish a reference model of the state of each agent

$$\dot{\bar{\omega}}_i = u_i(t) \tag{26}$$

where $\bar{\omega}_i$ is the state of the reference model corresponding to ω_i. According to (26), we can get (27) from (22)

$$u_{\omega i} = -f_i(\omega_i) - k\delta_i(t) + \dot{\bar{\omega}}_i \tag{27}$$

where δ_i is the tracking error of ω_i to $\bar{\omega}_i$, expressed as

$$\delta_i(t) = \omega_i(t) - \bar{\omega}_i(t). \tag{28}$$

The frequency controller designed above realizes the secondary frequency regulation in two parts. The first part is to realize the state ω_i of agent i tracking the state $\bar{\omega}_i$ of the reference model, i.e., $\lim_{t\to\infty}\delta_i(t) = 0$. The second part is to realize the convergence of the reference model state $\bar{\omega}_i$ and the frequency reference value ω_0 based on (26), i.e., $\lim_{t\to\infty}\bar{\omega}_i(t) - \omega_0 = 0$.

In order to reduce the number of communications between agents and save communication costs, the event-triggered communication considering time delay is used between agents. In (26), we designed the event-triggered distributed controller as

$$L + B = \begin{pmatrix} \sum\limits_{1\le j\le N}(a_{1j}) + b_1 & -a_{12} & \cdots & -a_{1j} & \cdots & -a_{1N} \\ -a_{21} & \sum\limits_{1\le j\le N}(a_{2j}) + b_2 & \cdots & -a_{2j} & \cdots & -a_{2N} \\ \vdots & \vdots & & \vdots & & \vdots \\ -a_{N1} & -a_{N2} & \cdots & -a_{Nj} & \cdots & \sum\limits_{1\le j\le N}(a_{Nj}) + b_N \end{pmatrix} \tag{17}$$

$$\begin{vmatrix} \sum\limits_{1\le j\le N}(a_{1j}) + b_1 - \varsigma & 0 & \cdots & 0 & \cdots & 0 \\ -a_{21} & \sum\limits_{1\le j\le N}(a_{2j}) + b_2 - \varsigma & \cdots & 0 & \cdots & 0 \\ \vdots & \vdots & & \vdots & & \vdots \\ -a_{N1} & -a_{N2} & \cdots & -a_{Nj} & \cdots & \sum\limits_{1\le j\le N}(a_{Nj}) + b_N - \varsigma \end{vmatrix}$$

$$= \prod_{1\le i\le N}\left(\sum_{1\le j\le N}(a_{ij}) + b_i - \varsigma\right) = 0. \tag{18}$$

(29). At this time, (26) and (29) constitute a control loop

$$u_i(t) = q_{\omega i}(t_k^i - \tau) + \varepsilon_i(\omega_i(t_k^i - \tau) - \bar{\omega}(t_k^i - \tau)) \quad (29)$$

where $\tau \geq 0$ denotes the time delay

$$q_{\omega i}(t) = \sum_{j=1}^{N} a_{ij}\left(\omega_j(t) - \omega_i(t)\right) + b_i\left(\omega_0 - \omega_i(t)\right). \quad (30)$$

The event-triggered time instants $\{t_k^i\}$ for agent i are declined by $t_{k+1}^i = \inf\{t > t_k^i, f_{\omega i}(t) > 0\}$, where $f_{\omega i}(t)$ is the event-triggered function. We design the event-triggered function $f_{\omega i}(t)$ as follows:

$$f_{\omega i}(t) = \|e_{\omega i}(t)\| - \beta_\omega e^{-\gamma_\omega(t-t_0)} \quad (31)$$

where $\beta_\omega > 0$, $\gamma_\omega > 0$, t_0 is the initial time and $e_{\omega i}(t) = q_{\omega i}(t_k^i) - q_{\omega i}(t)$. Let $\xi_{\omega i}(t) = \omega_i(t) - \omega_0(t)$, $\xi_\omega(t) = [\xi_{\omega 1}^T(t), \xi_{\omega 2}^T(t), \ldots, \xi_{\omega N}^T(t)]^T$, $e_\omega(t) = [e_{\omega 1}^T(t), e_{\omega 2}^T(t), \ldots, e_{\omega N}^T(t)]^T$. According to the above equations, we can get (32) from (30)

$$\dot{\xi}_\omega(t) = e_\omega(t - \tau) - [(L + B) \otimes I_n]\xi_\omega(t - \tau). \quad (32)$$

Equation (32) can be rewritten as

$$\dot{\xi}_\omega(t) = M_\omega \xi_\omega(t - \tau) + e_\omega(t - \tau) \quad (33)$$

where $M_\omega = -[(L + B) \otimes I_n]$.

The variables described above need to meet certain constraints to make the proposed controller stable. This constraint condition will be used in the proposed controller stability proof. Therefore, we make the following assumption for the above variables.

Assumption 3: We set

$$Z_\omega = \frac{-\gamma_\omega(\alpha - \gamma_\omega)\|\xi_\omega(t_0)\| - \|M_\omega\|\beta_\omega(1 - e^{\gamma_\omega\tau} - \gamma_\omega)}{(1 - e^{\gamma_\omega\tau})\|M_\omega\|\|M_\omega\|e^{\gamma_\omega\tau}}$$

there are $Z_\omega \geq \|\xi_\omega(t_0)\|$ and $0 < \gamma_\omega < \alpha$.

Different from the existing control methods VSG and GDC, such as [28], [29], [30], [32], the distributed control method based on event-triggered multiagent consistency is introduced into the proposed frequency secondary controller. This not only meets the need of frequency regulation, but also makes frequency secondary control more flexible.

D. Active Power Controller

Virtual governor is used to compensate the frequency in this article. The principle of virtual governor is to adjust the frequency by the power compensation $P_{\omega i}$, shown as (20). After introducing the virtual governor for secondary frequency control, the frequency dynamic (5) based on GDC can be written as

$$\frac{\omega_{ni} - \omega_i}{P_{seti} + P_{\omega i} - P_i} = -\frac{d_i s + e_i}{a_i s^2 + b_i s + c_i}. \quad (34)$$

When GDC with virtual governor is in stable state, there is

$$(P_{seti} + P_{\omega i} - P_i)e_i + c_i(\omega_{ni} - \omega_i) = 0. \quad (35)$$

Combining with (20), (35) can be rewritten as

$$(P_{seti} + P_{\omega i} - P_i)e_i = -c_i\frac{P_{\omega i}}{k_\omega}. \quad (36)$$

Further obtain

$$P_{mari} = P_{seti} - P_i = -\left(1 + \frac{c_i}{e_i k_\omega}\right)P_{\omega i} \quad (37)$$

where P_{mari} is the active power margin. We can choose appropriate c_i, e_i and frequency regulation factor k_ω to make $\frac{c_i}{e_i k_\omega} \gg 1$. Then, (37) can be simplified to

$$P_{seti} - P_i = -\frac{c_i}{e_i k_\omega}P_{\omega i}. \quad (38)$$

By selecting the same frequency regulation factor k_ω for all controllers, there must be the following relationship:

$$\lim_{t\to\infty} P_{\omega i} = \lim_{t\to\infty} P_{\omega j} \Rightarrow \lim_{t\to\infty} e_i\frac{P_{seti} - P_i}{c_i} = e_j\frac{P_{setj} - P_j}{c_j}. \quad (39)$$

Shown as (39), if we set the active power command P_{seti} as the rated power value of DG and $c_i = 1$, by selecting the coefficient $\frac{1}{e_i}$ of the same ratio with the rated power ratio, then the active power sharing will be obtained, i.e., the active power P_i with the same ratio. The following question is how to achieve the convergence of the active power compensation $P_{\omega i}$ to get the active power sharing. We designed the event-triggered distributed controller of the active power compensation based on the multiagent theory, shown as

$$u_{Pi} = q_{Pi}(t_k^i - \tau) \quad (40)$$

where

$$q_{Pi}(t) = \sum_{j=1}^{N} a_{ij}\left(P_{\omega j}(t) - P_{\omega i}(t)\right). \quad (41)$$

The event-triggered time instants $t_{k+1}^i = \inf\{t > t_k^i, f_{Pi}(t) > 0\}$, the event-triggered function $f_{Pi}(t)$ is designed as

$$f_{Pi}(t) = \|e_{Pi}(t)\| - \beta_P e^{-\gamma_P(t-t_0)} \quad (42)$$

where $\beta_P > 0$, $\gamma_P > 0$, $e_{Pi}(t) = q_{Pi}(t_k^i) - q_{Pi}(t)$, t_0 is the initial time.

Under the action of the controller (40), $\lim_{t\to\infty} P_{\omega i} = \lim_{t\to\infty} P_{\omega j}$, then the accurate active power sharing is achieved.

E. Voltage Controller

The voltage of DG, like the frequency, will deviate from the rated value under the influence of line impedance mismatch and load fluctuation. Therefore, we need to design a secondary voltage controller to regulate the voltage.

The system equation of MG based on inverter can be written as the following nonlinear system equation:

$$\begin{cases} \dot{x}_i = k(x_i) + f(x_i)D_i + r(x_i)u_{Ui} \\ y_i = w(x_i) \end{cases} \quad (43)$$

where the output $y_i = u_{odi}$ and control input $u_{Ui} = U_{ni}$. $k(x_i)$, $f(x_i)$, $r(x_i)$, and $w(x_i)$ are nonlinear functions of x_i, D_i is a known disturbance. Their detailed expressions can be extracted from [36, Section II-A].

For (43), we can get the relationship between the output y_i and the control input u_{Ui} after the second derivative of y_i as

$$\ddot{y}_i = L_{r_i}L_{F_i}w_i u_{Ui} + L_{F_i}^2 w_i \quad (44)$$

where

$$F_i(x_i) = f_i(x_i)D_i + k_i(x_i) \tag{45}$$

$L_{F_i}w_i$ is the Lie derivative of w_i with respect to F_i, there are

$$L_{F_i}w_i = \frac{\partial(w_i)}{\partial x_i}F_i \tag{46}$$

$$L_{F_i}^2 w_i = L_{F_i}(L_{F_i}w_i) = \frac{\partial(L_{F_i}w_i)}{\partial x_i}F_i. \tag{47}$$

We set the auxiliary control v_i as

$$v_i = L_{F_i}^2 w_i + L_{r_i}L_{F_i}w_i u_{Ui}. \tag{48}$$

By combining (48), (44) can be rewritten as

$$\ddot{y}_i = v_i. \tag{49}$$

By designing a suitable v_i, we can get the consistency of the output y_i. From (48), there is

$$u_{Ui} = (L_{r_i}L_{F_i}w_i)^{-1}(-L_{F_i}^2 w_i + v_i). \tag{50}$$

We set $\dot{y}_i(t) = g_i(t)$. Combining this equation, (51) can be deduced from

$$\begin{cases} \dot{y}_i(t) = g_i(t) \\ \dot{g}_i(t) = v_i(t), i = 1, 2, \ldots, N. \end{cases} \tag{51}$$

For the leader of the multiagent system, there is $\dot{y}_0(t) = g_0(t)$ and $\dot{g}_0(t) = 0$. In (49), we choose the $v_i(t)$ as

$$v_i(t) = q_{yi}(t_k^i - \tau) + q_{gi}(t_k^i - \tau) \tag{52}$$

where

$$q_{yi}(t) = \sum_{j=1}^{N} a_{ij}\left(y_j(t) - y_i(t)\right) + b_i\left(y_0(t) - y_i(t)\right) \tag{53}$$

$$q_{gi}(t) = \sum_{j=1}^{N} a_{ij}\left(g_j(t) - g_i(t)\right) + b_i\left(g_0(t) - g_i(t)\right). \tag{54}$$

The event-triggered time instants $t_{k+1}^i = \inf\{t > t_k^i, f_i(t) > 0\}$. We design the event-triggered function $f_i(t)$ as follows:

$$f_i(t) = \|e_{yi}(t)\| + \|e_{gi}(t)\| - \beta e^{-\gamma(t-t_0)} \tag{55}$$

where $\beta > 0$, $\gamma > 0$, $e_{yi}(t) = q_{yi}(t_k^i) - q_{yi}(t)$, and $e_{gi}(t) = q_{gi}(t_k^i) - q_{gi}(t)$. Let $\eta_i(t) = g_i(t) - g_0(t)$, $\xi_i(t) = y_i(t) - y_0(t)$, $\eta(t) = [\eta_1^T(t), \eta_2^T(t), \ldots, \eta_N^T(t)]^T$, $\xi(t) = [\xi_1^T(t), \xi_2^T(t), \ldots, \xi_N^T(t)]^T$, $e_g(t) = [e_{g1}^T(t), e_{g2}^T(t), \ldots, e_{gN}^T(t)]^T$, $e_y(t) = [e_{y1}^T(t), e_{y2}^T(t), \ldots, e_{yN}^T(t)]^T$. According to the above equations, we can get (56) from (51)

$$\begin{cases} \dot{\xi}(t) = \eta(t) \\ \dot{\eta}(t) = e_y(t-\tau) + e_g(t-\tau) - [(L+B)\otimes I_n]\,\eta(t-\tau) \\ \qquad - [(L+B)\otimes I_n]\,\xi(t-\tau) \end{cases} \tag{56}$$

then (56) can be rewritten as

$$\dot{\varepsilon}(t) = E_1\varepsilon(t) + M\varepsilon(t-\tau) + E_2(e_y(t-\tau) + e_g(t-\tau)) \tag{57}$$

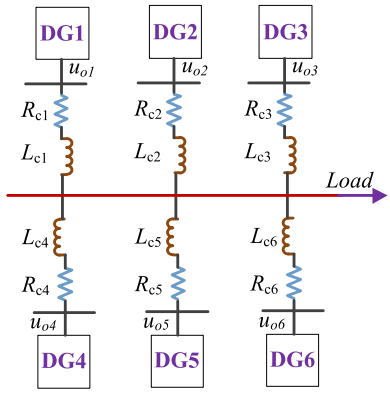

Fig. 3. Physical structure diagram of MG.

where $\varepsilon(t) = [\xi^T(t), \eta^T(t)]^T$, $E_1 = \begin{pmatrix} 0 & I_n \\ 0 & 0 \end{pmatrix}$, $E_2 = \begin{pmatrix} 0 & 0 \\ 0 & I_n \end{pmatrix}$, $M = \begin{pmatrix} 0 & 0 \\ -[(L+B)\otimes I_n] & -[(L+B)\otimes I_n] \end{pmatrix}$.

Similarly, the variables described above need to meet certain constraints to make the proposed controller stable. Therefore, we make the following assumption for the above variables.

Assumption 4: We set

$$Z = \frac{-\gamma(\alpha-\gamma)\,\|\varepsilon(t_0)\| - \|M\|\,\|E_2\|\,\beta\,(1 - e^{\gamma\tau} - \gamma)}{(1-e^{\gamma\tau})\,(\|M\|\,\|E_1\| + \|M\|\,\|M\|\,e^{\gamma\tau})}$$

there are $Z \geq \|\varepsilon(t_0)\|$ and $0 < \gamma < \alpha$.

III. Stability Analysis of the System

Theorem 1: Suppose Assumptions 1–3 hold, the frequency of each DG will be adjusted to the frequency reference value by the distributed frequency secondary controller (29), and there is no Zeno behavior.

Proof: Please see Appendix A for the detailed proof process. This means that the frequency of each DG will converge to the reference value. ■

The proof process of the stability of the active power controller is similar to that of the frequency controller, and will not be repeated here.

Theorem 2: Suppose Assumptions 1–2 and 4 hold, the voltage of each DG will be adjusted to the voltage reference value by the distributed voltage secondary controller (52), and there is no Zeno behavior.

Proof: Please see Appendix B for the detailed proof process. This means that the voltage of each DG will converge to the reference value. ■

IV. Simulation Validation

The physical structure and communication topology of MG are shown in Figs. 3 and 4. The simulation model consists of six DGs. We will use the model to verify the effectiveness of the method. The simulation tool used in this article is MATLAB/Simulink.

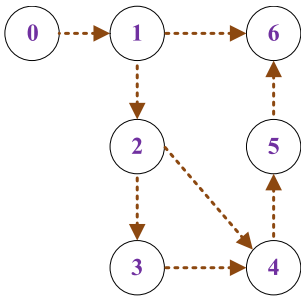

Fig. 4. Communication topology of MG.

TABLE I
SIMULATION PARAMETERS

DGs	DG1&DG2& DG3			DG4&DG5&DG6		
	$R_{f1,2,3}$	0.1Ω		$R_{f4,5,6}$	0.1Ω	
	$L_{f1,2,3}$	1.35 mH		$L_{f4,5,6}$	1.35 mH	
	$C_{f1,2,3}$	$50\mu F$		$C_{f4,5,6}$	$50\mu F$	
	$\tau_{11,2,3}$	0.78		$\tau_{14,5,6}$	0.78	
	$T_{11,2,3}$	4		$T_{14,5,6}$	4	
	$T_{21,2,3}$	0.1		$T_{24,5,6}$	0.17	
	$K_{1,2,3}$	5×10^{-5}		$K_{4,5,6}$	1×10^{-4}	
	$n_{1,2,3}$	1×10^{-4}		$n_{4,5,6}$	2×10^{-4}	
	$P_{set1,2,3}$	10kW		$P_{set4,5,6}$	5kW	
Lines	Line1		Line2		Line3	
	R_{c1}	0.1Ω	R_{c2}	0.15Ω	R_{c3}	0.2Ω
	L_{c1}	0.35 mH	L_{c2}	0.5 mH	L_{c3}	0.7 mH
	Line4		Line5		Line6	
	R_{c4}	0.08Ω	R_{c5}	0.05Ω	R_{c6}	0.3Ω
	L_{c4}	0.3 mH	L_{c5}	0.15 mH	L_{c6}	1.05 mH
Loads	P_{Load}		22kW			
	Q_{Load}		22kVar			
gain	k_ω		100			
	k		10			

The rated voltage value U_0 is 380 V, the rated value of angular frequency ω_0 is 100π(rad/s). Let $\beta = 11$, $\beta_\omega = 1$, $\beta_P = 2$, $\{\gamma = 0.1, \gamma_\omega = 0.5, \gamma_P = 0.3\} < \mathrm{Re}(\lambda_2(L+B))$. Time delay $\tau_{1,2} = 30$ ms, $\tau_{3,4} = 60$ ms, and $\tau_{5,6} = 90$ ms. Note that the delay time is usually more than ten milliseconds or tens of milliseconds [37], which meets the actual needs. The other simulation parameters are given in Table I. In addition, the parameters in Table I are selected according to the following principles. First, the selection of control parameters should meet Assumptions 3 and 4. Second the selection of relevant parameters of GDC controller is referred to [32]. Third, for the physical parameters of MG, such as rated voltage, rated frequency, line impedance value, and the value of *LC* filter, etc., their values refer to [38]. Finally, other parameters are obtained by trial-and-error method to make the whole system run stably.

We use four simulation examples to verify the effectiveness of the proposed controller. Case 1: Verify the secondary regulation capability of the controller. Since the traditional primary control method makes the frequency of MG deviate from the rated value, we first verify the regulation ability of the controller in this aspect. Case 2: Verify the plug-and-play capability of the proposed controller. Case 3: The superiority of the proposed control strategy is proved by comparing the proposed distributed GDC secondary control with distributed VSG secondary control and distributed droop control. Case 4: Verify the performance of the controller under communication interruption.

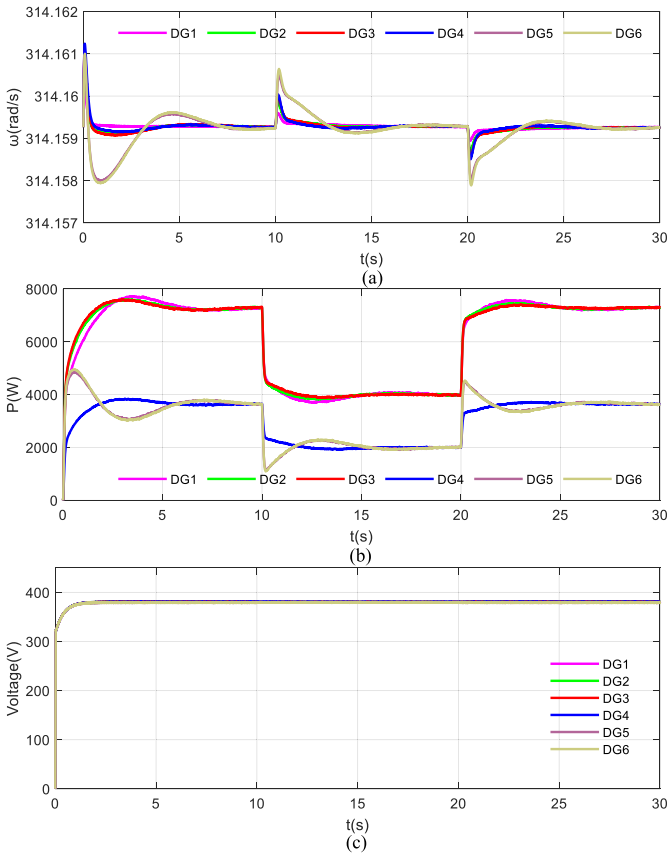

Fig. 5. Performance test of the proposed controller. (a) Frequency. (b) Active power. (c) Voltage.

A. Regulation Performance of the Controller

To verify the secondary regulation ability of the controller, by switching the load, we observe whether the frequency and voltage of MG can be stabilized at the rated values. When $t = 10$ s, we reduce the load by 10 kW. When $t = 20$ s, we restore the load. The total simulation time is 30 s. Shown as Fig. 5, when the load drops, the frequency of DG recovers to the rated value after a short oscillation. At this time, the power of each DG also decreases, but it keeps 2:2:1:1. When the load returns to the original value, the frequency will continue to operate stably at the rated value after a short adjustment. The active power remains shared. The fluctuation of the load has little effect on the voltage. The voltage of each DG is always stable at the rated value. Therefore, the control method proposed in this article solves the shortcomings of traditional droop control, and realizes the control objectives of power sharing and voltage and frequency secondary regulation.

The event-triggered communication method proposed in this article also reduces the number of communications between

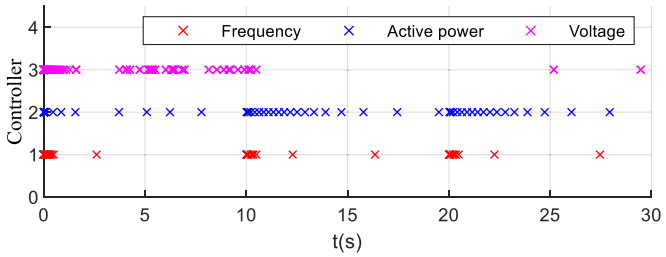

Fig. 6. Event trigger instants for DG1.

agents. The event-triggered time of frequency, voltage, and power communication of DG1 is shown in Fig. 6. When the load fluctuates, the communication mechanism of the agents is triggered, and the agents start to communicate. When the frequency, voltage, and power become stable, the communication between agents stops. Taking the controller of DG1 as an example, after calculation and comparison, when the event-triggered communication is not used, the communication times are 10^2 times more than that when the event-triggered communication is used. This control method greatly reduces the transmission of useless information. Therefore, this communication mechanism effectively reduces the number of communications between agents.

In addition, in order to fully verify the adjustment ability of the proposed controller, we observed the operation of MG by adjusting the load size under the maximum limit condition of DG. We take time delay as an example. Except for the time delay parameters, other parameters are selected according to Table I, and then the maximum time delay allowed by the system can be calculated as about 350 ms by using Assumptions 3 and 4. The simulation results are shown in Fig. 7. Shown as Fig. 7(a), when the delay time is less than 350 ms, the system can operate stably. Shown as Fig. 7(b) and (c), when the time delay is greater than 350 ms, the system becomes unstable and the operation curve oscillates. This reduces the quality of the power provided by MG. Therefore, the control method proposed in this article can provide a theoretical basis for the design of system parameters. The calculation and simulation of other parameters are similar to the above, and will not be repeated here.

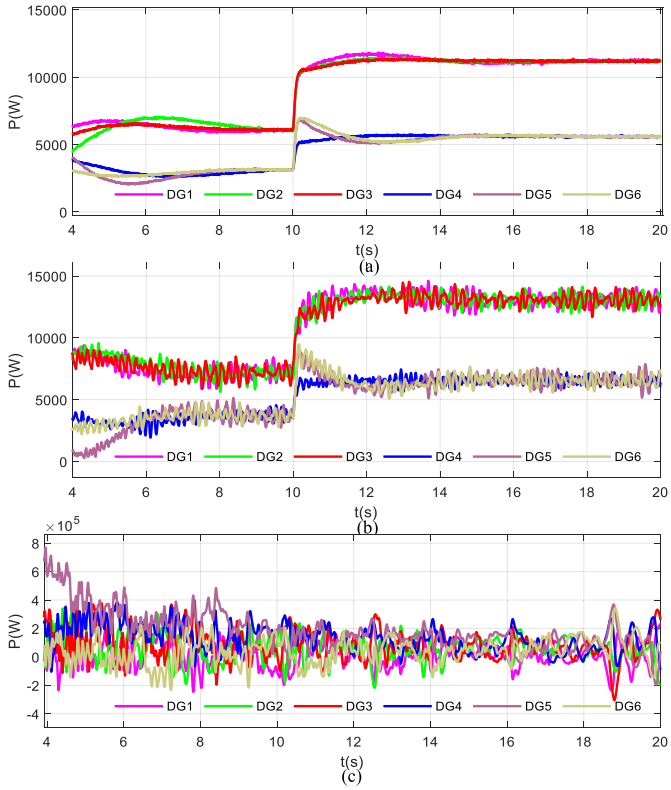

Fig. 7. Performance test under time delay limit conditions. (a) 300 ms. (b) 360 ms. (c) 400 ms.

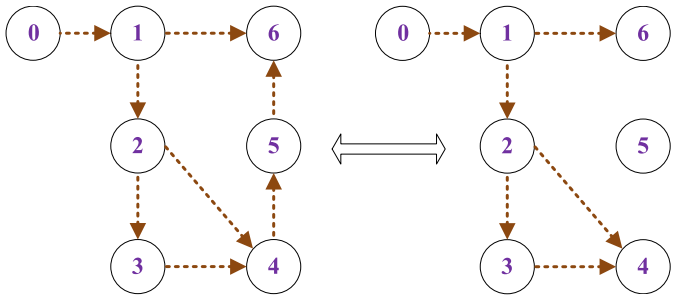

Fig. 8. Communication topology of MG.

B. Plug-and-Play

In this section, we will verify the plug-and-play capability of the proposed controller. By disconnecting and connecting DG5, we observe whether the frequency and voltage of MG can be stabilized at the rated values. The communication topology of MG is shown in Fig. 8. When $t = 10$ s, we disconnect DG5, and when $t = 20$ s, reconnect DG5. The total simulation time is 40 s. Shown in Fig. 9, when DG5 is disconnected, the frequency of DG recovers to the rated value after a short oscillation. At this time, the active power of DG5 is zero, and the active power of other DGs is still shared. The voltage of DG barely changes during this process. When DG5 is reconnected, DG5 suddenly starts to work from the no-load state, which causes the frequency to drop rapidly. It can be seen from the negative sign on the right side of (5) that the change direction of frequency and power is opposite. At this time, DG5 power generation rapidly increases. As the total load remains unchanged, the power generated by other DGs decreases. Then, the frequency and voltage continue to operate stably at the rated values after a short adjustment. The active power remains shared. Therefore, the control method proposed in this article has the plug-and-play ability. This makes the control of MG more flexible.

The event-triggered time of frequency, voltage, and power communication of DG1 is shown in Fig. 10. When the communication structure is switched, the communication mechanism of DGs is triggered, and the frequency controller, voltage controller, and power controller of DG1 start to communicate. When the system becomes stable, the communication between DGs stops. The trigger times of other DG controllers are similar to

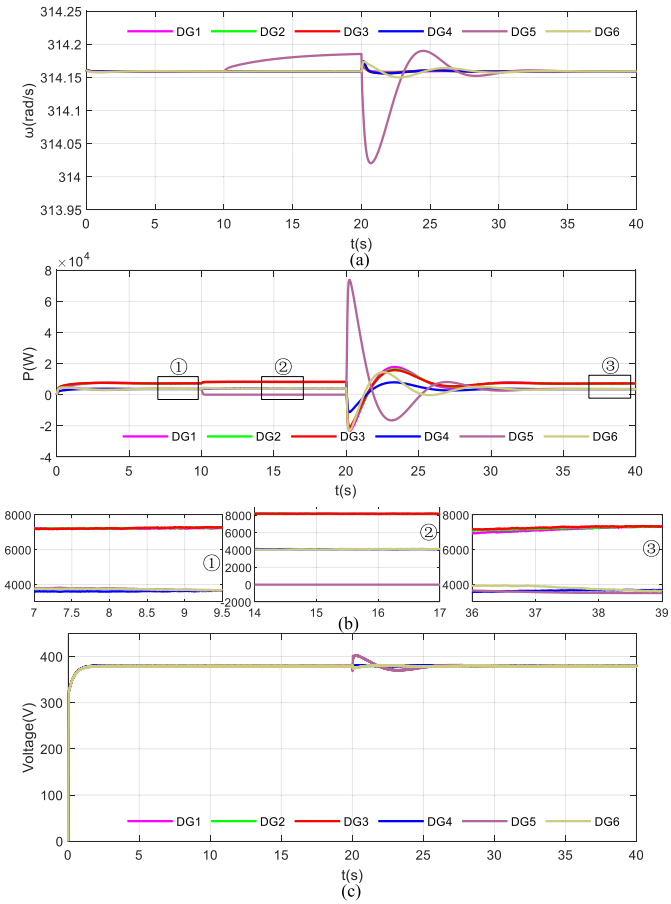

Fig. 9. Controller plug-and-play performance. (a) Frequency. (b) Active power. (c) Voltage.

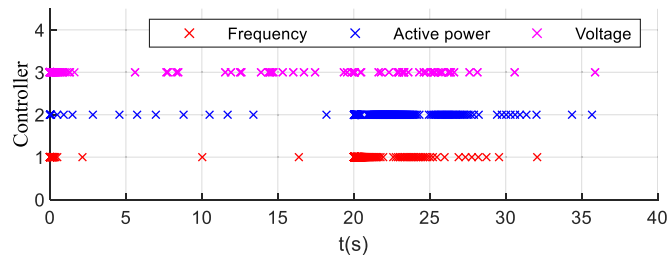

Fig. 10. Trigger time of DG1 communication.

those of DG1, but not all are given here. This communication mechanism effectively reduces the number of communications between DGs.

C. Performance Comparison of Different Controllers

In this section, we compare the proposed controller with distributed droop control [39] and distributed VSG control. In the distributed VSG control, VSG is used as the primary control. The distributed GDC control method proposed in this article is based on (5). Equation (5) is replaced by (4), and the same design process can be used to build the distributed VSG control. In the distributed secondary control based on VSG,

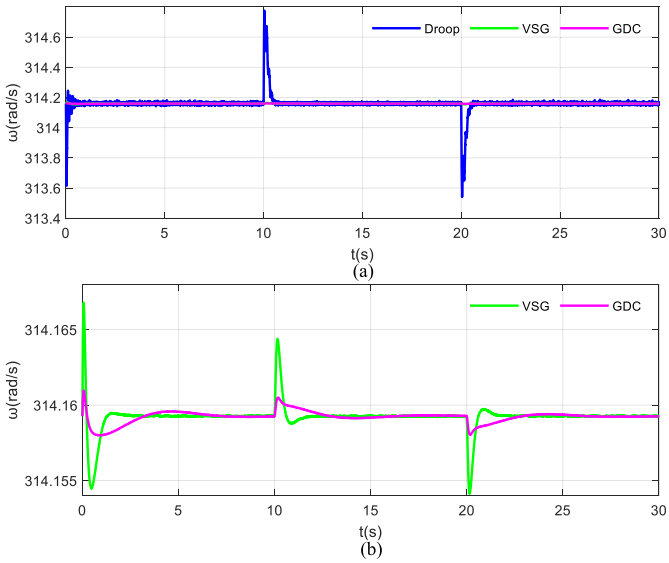

Fig. 11. Performance comparison of the controller under switching load. (a) Comparison of frequency response curve with distributed droop control [39] and distributed VSG control (b) Comparison of frequency response curve with distributed VSG.

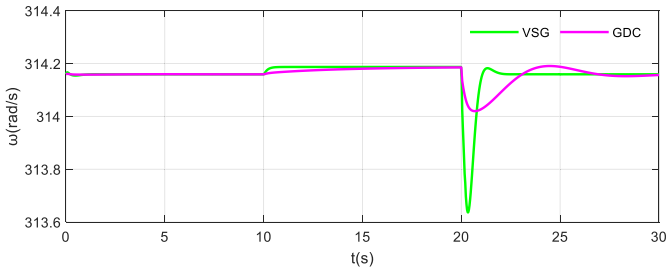

Fig. 12. Performance comparison of the controller under switching topology: comparison of frequency response curve with distributed VSG.

we select parameter values according to [32]. Taking DG5 as an example, let the inertia $J_5 = 32$ kg.m^2 and the damping coefficient $D_5 = 5000$. When $t = 10$ s, we reduce the load by 10 kW. When $t = 20$ s, we restore the load. The total simulation time is 30 s. The simulation results are shown in Fig. 11. As shown in Fig. 11(a), the droop control method does not have the ability to increase the system inertia. When the load fluctuates, the frequency curve using the droop control method fluctuates violently. Using the distributed VSG and GDC control method, the frequency fluctuation is greatly reduced.

In Fig. 11(b), comparing distributed GDC with distributed VSG, when the load fluctuates, the fluctuation peak of the frequency curve of DG5 using distributed GDC decreases and the degree of change of the curve slows down. Similarly, the plug-and-play simulation results of DG5 are shown in Fig. 12. When the communication topology of MG is changed, the frequency curve of the distributed VSG control method is obviously shaken, and the proposed method makes the frequency curve change more smoothly. Therefore, the simulation results show that the proposed control method is better than other methods in improving the inertia and damping characteristics of MG.

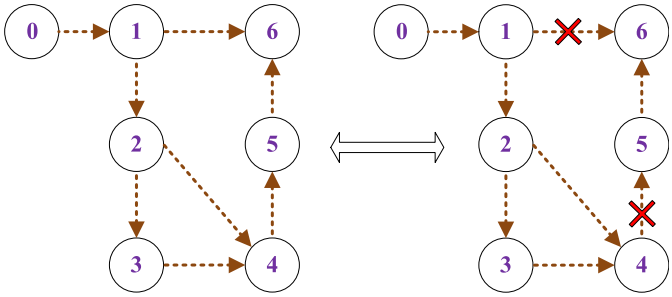

Fig. 13. Schematic diagram of communication interruption.

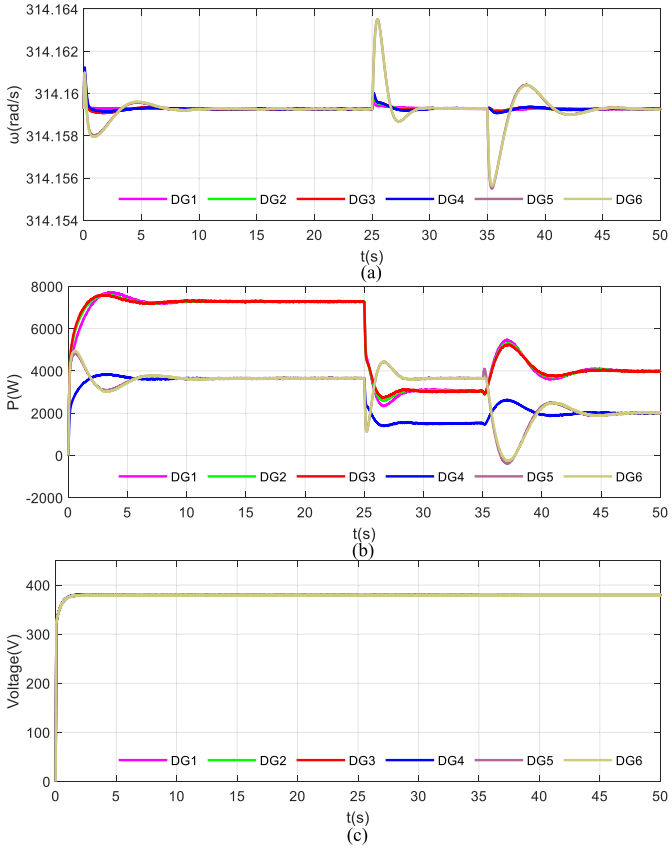

Fig. 14. Performance test of the controller under communication interruption. (a) Frequency. (b) Active power. (c) Voltage.

D. Performance Test of the Proposed Controller Under Communication Interruption

We analyze the influence of communication interruption on the controller in this section. When $t = 15$ s, the communication between DG1 and DG6 and between DG4 and DG5 is interrupted, shown as Fig. 13. When $t = 25$ s, we reduce the load by 10 kW. When $t = 35$ s, we restore the communication. The total simulation time is 50 s. The simulation results are shown in Fig. 14. As shown in Fig. 14, when the communication is interrupted at $t = 15$ s, since the MG is in the stable operation state at this time, there is no need for communication between the DGs, so the communication interruption has no impact on the operation of the MG. When the load changes, the original balance state of MG is broken, and the DG starts communication. The frequency of each DG is restored to the rated value after a short adjustment. Since DG5 and DG6 cannot communicate with other DGs at this time, their active power cannot be shared. The active power of other DGs still maintains power sharing. When the communication of MG is restored, the frequency of each DG is stabilized at the rated value after a short adjustment. At this time, the active power of each DG is restored to the state of power sharing. It can be seen from the figure that the communication interruption has little effect on the voltage. Simulation results show that the proposed control method has a certain ability to resist communication interruption.

Note that the microgrid simulation structure used in this article is an equivalent simulation model, which is equivalent to the load at a point [40]. However, the line impedance at the output end of DG is different, which means that the distance between DG and load is different. Therefore, the simulation structure adopted in this article is as universal as other simulation structures [15].

V. Conclusion

This article presented an event-triggered control strategy of distributed GDC considering time delay. The distributed GDC frequency secondary controller is constructed by using heterogeneous multiagent theory, which avoids complex parameter design. This method can not only adjust the frequency and realize active power sharing, but also make MG have inertia and damping characteristics. The distributed voltage controller realizes the secondary regulation of voltage. Using event-triggered communication can effectively reduce the number of communications. The stability of the proposed event-triggered controller is strictly proved and the Zeno behavior does not occur. The complicated Lyapunov equation of the system is avoided in the proof process. Simulation results show the effectiveness of the method.

In addition, the research group where the author works is currently building an experimental platform of MG, but the experimental platform has not been completed, and part of the experimental equipment is still lacking, so the conditions for experimental verification are not yet available. The combination of simulation and experimental verification can fully verify the effectiveness of the controller, which will be the focus of the research group in the future.

Appendix

A. Proof of Theorem 1

Proof: Combining (22) and (27), the derivative of (28) can be obtained

$$\begin{aligned}\dot{\delta}_i(t) &= \dot{\omega}_i(t) - \dot{\bar{\omega}}_i(t)\\ &= f_i(\omega_i) + u_{\omega i} - \dot{\bar{\omega}}_i(t)\\ &= -k\delta_i. \end{aligned} \tag{58}$$

The equation of the tracking error controller is simple, so we can directly use the simple Lyapunov equation to prove its stability. Let

$$V_\omega(t) = \frac{1}{2}\delta^T(t)\delta(t). \tag{59}$$

Then, we can get the derivative of (59) with respect to the tracking error δ, as

$$\dot{V}_\omega(t) = \delta^T(-k\delta) = -k\delta^2 \le 0. \tag{60}$$

Note that the above equation (60) is equal to zero if and only if δ is zero. This means that $\lim_{t\to\infty}\delta_i(t) = 0$. Therefore, there must be

$$\lim_{t\to\infty}\omega_i(t) = \bar{\omega}_i(t). \tag{61}$$

■

The frequency controller realizes the secondary frequency regulation in two steps. The first step is to realize the state ω_i of agent$i$ tracking the state $\bar{\omega}_i$ of the reference model. This step has been completed. The second step is to realize the convergence of the reference model state $\bar{\omega}_i$ and the frequency reference value ω_0. The second step will be demonstrated below.

Using Newton–Leibniz formula, we obtain

$$\begin{aligned}\xi_\omega(t-\tau) &= \xi_\omega(t) - \int_{t-\tau}^{t}\dot{\xi}_\omega(s)\mathrm{d}s \\ &= \xi_\omega(t) - \int_{t-\tau}^{t} M_\omega\xi_\omega(s-\tau)\mathrm{d}s \\ &\quad - \int_{t-\tau}^{t} e_\omega(s-\tau)\mathrm{d}s.\end{aligned} \tag{62}$$

There is

$$\begin{aligned}\dot{\xi}_\omega(t) = M_\omega\xi_\omega(t) - M_\omega\textstyle\int_{t-\tau}^{t}(M_\omega\xi_\omega(s-\tau) \\ + e_\omega(s-\tau))ds + e_\omega(t-\tau).\end{aligned} \tag{63}$$

Solving the differential equation (63) yields

$$\begin{aligned}\xi_\omega(t) &= e^{M_\omega(t-t_0)}\xi_\omega(t_0) \\ &\quad - \int_{t_0}^{t} e^{M_\omega(t-s)}M_\omega\left\{\int_{s-\tau}^{s}(M_\omega\xi_\omega(z-\tau)\right. \\ &\quad \left.+e_\omega(z-\tau))\,\mathrm{d}z - e_\omega(s-\tau)\right\}\mathrm{d}s.\end{aligned} \tag{64}$$

Equation (64) can be further deduced by using the properties of the eigenvalue of matrix in graph theory. Using Lemma 1 and *Lemma 2*, we can easily get $\mathrm{Re}(\lambda_N(M_\omega)) < 0$. So there are $\kappa \ge 1$ and $\alpha > 0$ for (65) to be true

$$\begin{aligned}\|\xi_\omega(t)\| &\le \kappa e^{-\alpha(t-t_0)}\|\xi_\omega(t_0)\| \\ &\quad + \kappa\int_{t_0}^{t} e^{-\alpha(t-s)}\|M_\omega\|\left\{\int_{s-\tau}^{s}\|M_\omega\|\,\|\xi_\omega(z-\tau)\|\right. \\ &\quad \left.+\|e_\omega(z-\tau)\|\,\mathrm{d}z + \|e_\omega(s-\tau)\|\right\}\mathrm{d}s.\end{aligned} \tag{65}$$

Combined with the event-trigged function $\|e_\omega(t-\tau)\| \le \beta_\omega e^{-\gamma_\omega(t-t_0)}$ and (65), we can get

$$\begin{aligned}\|\xi_\omega(t)\| &\le \kappa e^{-\alpha(t-t_0)}\|\xi_\omega(t_0)\| \\ &\quad + \kappa\int_{t_0}^{t} e^{-\alpha(t-s)}\left\{\int_{s-\tau}^{s}\|M_\omega\|^2\|\xi_\omega(z-\tau)\|\right. \\ &\quad \left.+\|M_\omega\|\,\beta_\omega e^{-\gamma_\omega(z-t_0)}\mathrm{d}z + \|M_\omega\|\,\beta_\omega e^{-\gamma_\omega(s-t_0)}\right\}\mathrm{d}s \\ &= \kappa e^{-\alpha(t-t_0)}\|\xi_\omega(t_0)\| \\ &\quad + \kappa\int_{t_0}^{t} e^{-\alpha(t-s)}\left\{\int_{s-\tau}^{s}\|M_\omega\|^2\|\xi_\omega(z-\tau)\|\,\mathrm{d}z\right\}\mathrm{d}s \\ &\quad + \kappa\int_{t_0}^{t} e^{-\alpha(t-s)}\left(\int_{s-\tau}^{s}\|M_\omega\|\,\beta_\omega e^{-\gamma_\omega(z-t_0)}\mathrm{d}z\right)\mathrm{d}s \\ &\quad + \kappa\int_{t_0}^{t} e^{-\alpha(t-s)}\|M_\omega\|\,\beta_\omega e^{-\gamma_\omega(s-t_0)}\mathrm{d}s.\end{aligned} \tag{66}$$

Further obtained

$$\begin{aligned}\|\xi_\omega(t)\| &\le \kappa e^{-\alpha(t-t_0)}\|\xi_\omega(t_0)\| \\ &\quad + \kappa\int_{t_0}^{t} e^{-\alpha(t-s)}\left\{\int_{s-\tau}^{s}\|M_\omega\|^2\|\xi_\omega(z-\tau)\|\,\mathrm{d}z\right\}\mathrm{d}s \\ &\quad + \frac{\kappa\|M_\omega\|\,\beta_\omega}{-\gamma_\omega(\alpha-\gamma_\omega)}(1 - e^{\gamma_\omega\tau} - \gamma_\omega) \\ &\quad \times\left(e^{-\gamma_\omega(t-t_0)} - e^{-\alpha(t-t_0)}\right).\end{aligned} \tag{67}$$

In order to prove the convergence of the system (30), the following equation can be proved:

$$\|\xi_\omega(t)\| \le \eta_\omega Z_\omega e^{-\gamma_\omega(t-t_0)} \tag{68}$$

where $\eta_\omega > 1$. Substituting (68) into (67) yields

$$\begin{aligned}&\|\xi_\omega(t)\| \\ &\le \kappa e^{-\alpha(t-t_0)}\|\xi_\omega(t_0)\| \\ &\quad + \kappa\int_{t_0}^{t} e^{-\alpha(t-s)}\left\{\int_{s-\tau}^{s}\|M_\omega\|^2\eta_\omega Z_\omega e^{-\gamma_\omega(z-\tau-t_0)}\mathrm{d}z\right\}\mathrm{d}s \\ &\quad + \frac{\kappa\|M_\omega\|\,\beta_\omega}{-\gamma_\omega(\alpha-\gamma_\omega)}(1 - e^{\gamma_\omega\tau} - \gamma_\omega) \\ &\quad \times\left(e^{-\gamma_\omega(t-t_0)} - e^{-\alpha(t-t_0)}\right).\end{aligned} \tag{69}$$

If Inequality (68) does not hold, there must be $t^* \ge t_0$ so that $\eta_\omega\kappa Z_\omega e^{-\gamma_\omega(t^*-t_0)} < \|\xi_\omega(t^*)\|$. When $t = t^*$, Inequality (69) can be written as

$$\begin{aligned}&\|\xi_\omega(t^*)\| \\ &\le \kappa e^{-\alpha(t^*-t_0)}\|\xi_\omega(t_0)\| \\ &\quad + \kappa\int_{t_0}^{t^*} e^{-\alpha(t^*-s)}\left\{\int_{s-\tau}^{s}\|M_\omega\|^2\eta_\omega Z_\omega e^{-\gamma_\omega(z-\tau-t_0)}\mathrm{d}z\right\}\mathrm{d}s\end{aligned}$$

$$
\begin{aligned}
&+\frac{\kappa\left\|M_\omega\right\|\beta_\omega}{-\gamma_\omega\left(\alpha-\gamma_\omega\right)}\left(1-e^{\gamma_\omega\tau}-\gamma_\omega\right)\\
&\times\left(e^{-\gamma_\omega(t^*-t_0)}-e^{-\alpha(t^*-t_0)}\right)\\
\leq&\left(\frac{\kappa\eta_\omega Z_\omega\left(1-e^{\gamma_\omega\tau}\right)\left\|M_\omega\right\|^2 e^{\gamma_\omega\tau}}{-\gamma_\omega\left(\alpha-\gamma_\omega\right)}\right.\\
&\left.+\frac{\kappa\eta_\omega\left\|M_\omega\right\|\beta_\omega\left(1-e^{\gamma_\omega\tau}-\gamma_\omega\right)}{-\gamma_\omega\left(\alpha-\gamma_\omega\right)}\right)e^{-\gamma_\omega(t^*-t_0)}\\
&+\left(\kappa\eta_\omega\left\|\xi_\omega\left(t_0\right)\right\|+\frac{\kappa\eta_\omega Z_\omega\left(1-e^{\gamma_\omega\tau}\right)\left(\left\|M_\omega\right\|\left\|M_\omega\right\|e^{\gamma_\omega\tau}\right)}{\gamma_\omega\left(\alpha-\gamma_\omega\right)}\right.\\
&\left.-\frac{\kappa\eta_\omega\left\|M_\omega\right\|\beta_\omega\left(1-e^{\gamma_\omega\tau}-\gamma_\omega\right)}{-\gamma_\omega\left(\alpha-\gamma_\omega\right)}\right)e^{-\alpha(t^*-t_0)}. \qquad (70)
\end{aligned}
$$

According to Assumption 3, we can get

$$
\begin{aligned}
\eta_\omega\kappa Z_\omega e^{-\gamma_\omega(t^*-t_0)}&<\left\|\xi_\omega\left(t^*\right)\right\|\\
&<\eta_\omega\kappa\left\|\xi_\omega\left(t_0\right)\right\|e^{-\gamma_\omega(t^*-t_0)}\\
&<\eta_\omega\kappa Z_\omega e^{-\gamma_\omega(t^*-t_0)}. \qquad (71)
\end{aligned}
$$

So Inequality (68) is true. This means that the consistency of the distributed frequency controller can converge exponentially.

The Dini derivative of $\|e_i(t)\|$ satisfies the following relationship:

$$
D^+\left\|e_i(t)\right\|=\frac{d}{dt}\sqrt{e_i^T(t)e_i(t)}\leq\left\|\dot{e}_i(t)\right\|. \qquad (72)
$$

Substituting (30) and (31) into (72) yields

$$
\begin{aligned}
&D^+\left\|e_{\omega i}(t)\right\|\\
&\leq\left\|\dot{e}_{\omega i}(t)\right\|\\
&\leq\|L+B\|^2\left\|\xi_\omega\left(t_k^i-\tau\right)\right\|+\|L+B\|\beta_\omega e^{-\gamma_\omega\left(t_k^i-\tau-t_0\right)}\\
&\quad+\|L+B\|^2\left\|\xi_\omega(t-\tau)\right\|+\|L+B\|\beta_\omega e^{-\gamma_\omega(t-\tau-t_0)}\\
&\leq\|L+B\|Z_\omega e^{-\gamma_\omega\left(t_k^i-t_0\right)}+\|L+B\|Z_\omega e^{-\gamma_\omega(t-t_0)}\\
&\quad+\left(2\|L+B\|^2Z_\omega+\|L+B\|\beta_\omega\right)\left(e^{-\gamma_\omega(t-\tau-t_0)}\right.\\
&\quad\left.+e^{-\gamma_\omega\left(t_k^i-\tau-t_0\right)}\right). \qquad (73)
\end{aligned}
$$

At the event-triggered instant $t=t_k^i$, $e_{\omega i}(t)$ will be reset to 0. From (73), we can obtain

$$
\begin{aligned}
\left\|e_{\omega i}(t)\right\|\leq&\left(\frac{e^{\gamma_\omega\tau}\left(2\|L+B\|^2Z_\omega+\|L+B\|\beta_\omega\right)}{\gamma_\omega}\right.\\
&\left.+\frac{\|L+B\|Z_\omega}{\gamma_\omega}\right)\left(e^{-\gamma_\omega\left(t_k^i-t_0\right)}-e^{-\gamma_\omega(t-t_0)}\right)\\
&+\left(\|L+B\|Z_\omega+e^{\gamma_\omega\tau}\left(2\|L+B\|^2Z_\omega\right.\right.\\
&\left.\left.+\|L+B\|\beta_\omega\right)\right)e^{-\gamma_\omega\left(t_k^i-t_0\right)}\left(t-t_k^i\right) \qquad (74)
\end{aligned}
$$

where $t\in[t_k^i,t_{k+1}^i]$, when the event-triggered function (31) is triggered, there is

$$
\beta_\omega e^{-\gamma_\omega(t-t_0)}<\left\|e_{\omega i}(t)\right\|. \qquad (75)
$$

According to (75), the next event will be triggered at the zero crossing of (31), and there is

$$
\begin{aligned}
&\beta_\omega e^{-\gamma_\omega\left(t_{k+1}^i-t_0\right)}\\
&<\left(\frac{e^{\gamma_\omega^\tau}\left(2\|L+B\|^2Z_\omega+\|L+B\|\beta_\omega\right)}{\gamma_\omega}\right.\\
&\quad\left.+\frac{\|L+B\|Z_\omega}{\gamma_\omega}\right)\left(e^{-\gamma_\omega\left(t_k^i-t_0\right)}-e^{-\gamma_\omega\left(t_{k+1}^i-t_0\right)}\right)\\
&\quad+\left(\|L+B\|Z_\omega+e^{\gamma_\omega\tau}\left(2\|L+B\|^2Z_\omega\right.\right.\\
&\quad\left.\left.+\|L+B\|\beta_\omega\right)\right)e^{-\gamma_\omega\left(t_k^i-t_0\right)}\left(t_{k+1}^i-t_k^i\right). \qquad (76)
\end{aligned}
$$

Let $T_k^i=t_{k+1}^i-t_k^i$, there is

$$
\begin{aligned}
\beta_\omega e^{-\gamma_\omega T_k^i}<&\left(\frac{e^{\gamma_\omega\tau}\left(2\|L+B\|^2Z_\omega+\|L+B\|\beta_\omega\right)}{\gamma_\omega}\right.\\
&\left.+\frac{\|L+B\|Z_\omega}{\gamma_\omega}\right)\left(1-e^{-\gamma_\omega T_k^i}\right)\\
&+\left(\|L+B\|Z_\omega+e^{\gamma_\omega\tau}\left(2\|L+B\|^2Z_\omega\right.\right.\\
&\left.\left.+\|L+B\|\beta_\omega\right)\right)T_k^i. \qquad (77)
\end{aligned}
$$

Since the right side of (77) is greater than zero, (78) must be true

$$
T_k^i>0. \qquad (78)
$$

Therefore, the frequency controller does not have Zeno behavior.

B. Proof of Theorem 2

Proof: Using the Newton–Leibnitz formula, we obtain

$$
\begin{aligned}
\varepsilon(t-\tau)&=\varepsilon(t)-\int_{t-\tau}^{t}\dot{\varepsilon}(s)ds\\
&=\varepsilon(t)-\int_{t-\tau}^{t}E_1\varepsilon(s)ds-\int_{t-\tau}^{t}M\varepsilon(s-\tau)ds\\
&\quad-\int_{t-\tau}^{t}E_2\left(e_y(s-\tau)+e_g(s-\tau)\right)ds. \qquad (79)
\end{aligned}
$$

Then, we have

$$
\begin{aligned}
\dot{\varepsilon}(t)=&\left(E_1+M\right)\varepsilon(t)-M\int_{t-\tau}^{t}E_1\varepsilon(s)+M\varepsilon(s-\tau)\\
&+E_2\left(e_y(s-\tau)+e_g(s-\tau)\right)ds\\
&+E_2\left(e_y(t-\tau)+e_g(t-\tau)\right). \qquad (80)
\end{aligned}
$$

Solving differential equation (80), there is

$$\begin{aligned}\varepsilon(t) = {} & e^{(E_1+M)(t-t_0)}\varepsilon(t_0) \\ & - \int_{t_0}^{t} e^{(E_1+M)(t-s)} M \left\{ \int_{s-\tau}^{s} E_1\varepsilon(z) \right. \\ & + M\varepsilon(z-\tau) + E_2\left(e_y(z-\tau)+e_g(z-\tau)\right)dz \\ & \left. -E_2\left(e_y(s-\tau)+e_g(s-\tau)\right)\right\} ds. \end{aligned} \tag{81}$$

Similar to the proof process of Theorem 1, the property of matrix eigenvalue is also used to further deduce (81). Using *Lemma 3*, we can easily get $\mathrm{Re}(\lambda_N(E_1+M)) < 0$. So there are $\kappa \geq 1$ and $\alpha > 0$ that make (82) hold

$$\begin{aligned} & \|\varepsilon(t)\| \\ & \leq \kappa e^{-\alpha(t-t_0)} \|\varepsilon(t_0)\| \\ & \quad + \kappa \int_{t_0}^{t} e^{-\alpha(t-s)} \|M\| \left\{ \int_{s-\tau}^{s} \|E_1\| \, \|\varepsilon(z)\| \right. \\ & \quad + \|M\| \|\varepsilon(z-\tau)\| + \|E_2\| \, \|e_y(z-\tau)+e_g(z-\tau)\| \, dz \\ & \quad \left. + \|E_2\| \, \|e_y(s-\tau)+e_g(s-\tau)\| \right\} ds. \end{aligned} \tag{82}$$

Combining the event-triggered function $\|e_y(t-\tau)\| + \|e_g(t-\tau)\| \leq \beta e^{-\gamma(t-t_0)}$ and (82), we can obtain

$$\begin{aligned} & \|\varepsilon(t)\| \\ & \leq \kappa e^{-\alpha(t-t_0)} \|\varepsilon(t_0)\| \\ & \quad + \kappa \int_{t_0}^{t} e^{-\alpha(t-s)} \left\{ \int_{s-\tau}^{s} \|E_1\| \, \|M\| \|\varepsilon(z)\| \right. \\ & \quad + \|M\|^2 \|\varepsilon(z-\tau)\| + \|E_2\| \, \|M\| \beta e^{-\gamma(z-t_0)} dz \\ & \quad \left. + \|M\| \, \|E_2\| \, \beta e^{-\gamma(s-t_0)} \right\} ds \\ & = \kappa e^{-\alpha(t-t_0)} \|\varepsilon(t_0)\| \\ & \quad + \kappa \int_{t_0}^{t} e^{-\alpha(t-s)} \left\{ \int_{s-\tau}^{s} \|E_1\| \, \|M\| \|\varepsilon(z)\| dz \right. \\ & \quad \left. + \int_{s-\tau}^{s} \|M\|^2 \|\varepsilon(z-\tau)\| dz \right\} ds \\ & \quad + \kappa \int_{t_0}^{t} e^{-\alpha(t-s)} \left(\int_{s-\tau}^{s} \|E_2\| \, \|M\| \beta e^{-\gamma(z-t_0)} dz \right) ds \\ & \quad + \kappa \int_{t_0}^{t} e^{-\alpha(t-s)} \|E_2\| \, \|M\| \beta e^{-\gamma(s-t_0)} ds. \end{aligned} \tag{83}$$

Finally, there is

$$\begin{aligned} \|\varepsilon(t)\| \leq {} & \kappa e^{-\alpha(t-t_0)} \|\varepsilon(t_0)\| \\ & + \kappa \int_{t_0}^{t} e^{-\alpha(t-s)} \left\{ \int_{s-\tau}^{s} \|M\| \, \|E_1\| \, \|\varepsilon(z)\| dz \right. \\ & \left. + \int_{s-\tau}^{s} \|M\|^2 \|\varepsilon(z-\tau)\| dz \right\} ds \\ & + \frac{\kappa \|M\| \, \|E_2\| \, \beta}{-\gamma(\alpha-\gamma)} \left(1 - e^{\gamma\tau} - \gamma\right) \left(e^{-\gamma(t-t_0)} \right. \\ & \left. - e^{-\alpha(t-t_0)} \right). \end{aligned} \tag{84}$$

■

In order to prove that the voltage distributed controller (52) can converge, the following equation can be proved to be true:

$$\|\varepsilon(t)\| \leq \eta Z e^{-\gamma(t-t_0)} \tag{85}$$

where $\eta > 1$. Substituting (85) into (84) yields

$$\begin{aligned} & \|\varepsilon(t)\| \\ & \quad \leq \kappa e^{-\alpha(t-t_0)} \|\varepsilon(t_0)\| \\ & \quad + \kappa \int_{t_0}^{t} e^{-\alpha(t-s)} \left\{ \int_{s-\tau}^{s} \|M\| \, \|E_1\| \, \eta Z e^{-\gamma(z-t_0)} dz \right. \\ & \quad \left. + \int_{s-\tau}^{s} \|M\|^2 \eta Z e^{-\gamma(z-\tau-t_0)} dz \right\} ds \\ & \quad + \frac{\kappa \|M\| \, \|E_2\| \, \beta}{-\gamma(\alpha-\gamma)} \left(1 - e^{\gamma\tau} - \gamma\right) \left(e^{-\gamma(t-t_0)} \right. \\ & \quad \left. - e^{-\alpha(t-t_0)} \right). \end{aligned} \tag{86}$$

If Inequality (85) does not hold, there must be $t^* \geq t_0$ for $\eta\kappa Z e^{-\gamma(t^*-t_0)} < \|\varepsilon(t^*)\|$. When $t = t^*$, Inequality (86) can be written as

$$\begin{aligned} & \|\varepsilon(t^*)\| \\ & \leq \kappa e^{-\alpha(t^*-t_0)} \|\varepsilon(t_0)\| \\ & \quad + \kappa \int_{t_0}^{t^*} e^{-\alpha(t^*-s)} \left\{ \int_{s-\tau}^{s} \|M\| \, \|E_1\| \, \eta Z e^{-\gamma(z-t_0)} dz \right. \\ & \quad \left. + \int_{s-\tau}^{s} \|M\|^2 \eta Z e^{-\gamma(z-\tau-t_0)} dz \right\} ds \\ & \quad + \frac{\kappa \|M\| \, \|E_2\| \, \beta}{-\gamma(\alpha-\gamma)} \left(1 - e^{\gamma\tau} - \gamma\right) \left(e^{-\gamma(t^*-t_0)} - e^{-\alpha(t^*-t_0)} \right) \\ & \leq \frac{1}{-\gamma(\alpha-\gamma)} \left(\kappa\eta Z \left(1 - e^{\gamma\tau}\right) \left(\|M\| \, \|E_1\| + \|M\|^2 e^{\gamma\tau}\right) \right. \\ & \quad + \kappa\eta \|M\| \, \|E_2\| \, \beta \left(1 - e^{\gamma\tau} - \gamma\right)) e^{-\gamma(t^*-t_0)} + (\kappa\eta \|\varepsilon(t_0)\| \\ & \quad - \frac{1}{-\gamma(\alpha-\gamma)} \left(\kappa\eta Z \left(1 - e^{\gamma\tau}\right) \left(\|M\| \, \|E_1\| + \|M\|^2 e^{\gamma\tau}\right) \right. \\ & \quad \left. + \kappa\eta \|M\| \, \|E_2\| \, \beta \left(1 - e^{\gamma\tau} - \gamma\right)) e^{-\alpha(t^*-t_0)}. \end{aligned} \tag{87}$$

According to *Assumption 4*, we can conclude that

$$\begin{aligned}\eta\kappa Z e^{-\gamma(t^*-t_0)} &< \|\varepsilon(t^*)\| \\ &< \eta\kappa \|\varepsilon(t_0)\| e^{-\gamma(t^*-t_0)} \\ &< \eta\kappa Z e^{-\gamma(t^*-t_0)}. \end{aligned} \tag{88}$$

So Inequality (85) is true. This means that the consistency of the distributed voltage controller can converge exponentially. The following will prove that the controller has no Zeno behavior.

Substituting (53)–(55) into (72) yields

$$\begin{aligned} & D^+ \|e_{yi}(t) + e_{gi}(t)\| \\ & \le \|\dot{e}_{yi}(t) + \dot{e}_{gi}(t)\| \\ & \le \|L+B\| \left\|\eta\left(t_k^i\right)\right\| + \|L+B\|^2 \left\|\xi\left(t_k^i - \tau\right)\right\| \\ & \quad + \|L+B\|\|\eta(t)\| + \|L+B\|\beta e^{-\gamma\left(t_k^i-\tau-t_0\right)} \\ & \quad + \|L+B\|^2 \left\|\eta\left(t_k^i-\tau\right)\right\| + \|L+B\|^2\|\eta(t-\tau)\| \\ & \quad + \|L+B\|^2\|\xi(t-\tau)\| + \|L+B\|\beta e^{-\gamma(t-\tau-t_0)} \\ & \le \|L+B\| Z e^{-\gamma\left(t_k^i-t_0\right)} + \|L+B\| Z e^{-\gamma(t-t_0)} \\ & \quad + \left(2\|L+B\|^2 Z + \|L+B\|\beta\right)\left(e^{-\gamma(t-\tau-t_0)}\right. \\ & \quad \left. + e^{-\gamma\left(t_k^i-\tau-t_0\right)}\right). \end{aligned} \tag{89}$$

At the event-triggered instant $t = t_k^i$, $e_i(t)$ will be reset to 0. Through (89), we can get

$$\begin{aligned} \|e_i(t)\| \le \frac{1}{\gamma} & \left(\|L+B\| Z + e^{\gamma\tau}\left(2\|L+B\|^2 Z\right.\right. \\ & \left.\left. + \|L+B\|\beta\right)\right)\left(e^{-\gamma\left(t_k^i-t_0\right)} - e^{-\gamma(t-t_0)}\right) \\ & + \left(\|L+B\| Z + e^{\gamma\tau}\left(2\|L+B\|^2 Z\right.\right. \\ & \left.\left. + \|L+B\|\beta\right)\right) e^{-\gamma\left(t_k^i-t_0\right)}\left(t - t_k^i\right) \end{aligned} \tag{90}$$

where $t \in [t_k^i, t_{k+1}^i]$. When the event-triggered function (55) is triggered, we obtain

$$\beta e^{-\gamma(t-t_0)} < \|e_{yi}(t)\| + \|e_{gi}(t)\|. \tag{91}$$

According to (91), the next event will be triggered when (55) crosses zero. We obtain

$$\begin{aligned} & \beta e^{-\gamma\left(t_{k+1}^i-t_0\right)} \\ & \le \frac{1}{\gamma}\left(\|L+B\| Z + e^{\gamma t}\left(2\|L+B\|^2 Z\right.\right. \\ & \quad \left.\left. + \|L+B\|\beta\right)\right)\left(e^{-\gamma\left(t_k^i-t_0\right)} - e^{-\gamma\left(t_{k+1}^i-t_0\right)}\right) \\ & \quad + \left(\|L+B\| Z + e^{\gamma\tau}\left(2\|L+B\|^2 Z\right.\right. \\ & \quad \left.\left. + \|L+B\|\beta\right)\right) e^{-\gamma\left(t_k^i-t_0\right)}\left(t_{k+1}^i - t_k^i\right). \end{aligned} \tag{92}$$

Let $T_k^i = t_{k+1}^i - t_k^i$, we have

$$\begin{aligned} \beta e^{-\gamma T_k^i} < \frac{1}{\gamma} & \left(\|L+B\| Z + e^{\gamma\tau}\left(2\|L+B\|^2 Z\right.\right. \\ & \left.\left. + \|L+B\|\beta\right)\right)\left(1 - e^{-\gamma T_k^i}\right) + \left(\|L+B\| Z\right. \\ & \left. + e^{\gamma t}\left(2\|L+B\|^2 Z + \|L+B\|\beta\right)\right) T_k^i. \end{aligned} \tag{93}$$

The right side of (93) is greater than zero, then Inequality (94) must be true

$$T_k^i > 0. \tag{94}$$

There's no Zeno behavior.

REFERENCES

[1] B. Liu, T. Wu, Z. Liu, and J. Liu, "A small-AC-signal injection-based decentralized secondary frequency control for droop-controlled islanded microgrids," *IEEE Trans. Power Electron.*, vol. 35, no. 11, pp. 11634–11651, Nov. 2020.

[2] V. Nasirian, Q. Shafiee, J. M. Guerrero, F. L. Lewis, and A. Davoudi, "Droop-free distributed control for AC microgrids," *IEEE Trans. Power Electron.*, vol. 31, no. 2, pp. 1600–1617, Feb. 2016.

[3] M. A. Awal, H. Yu, H. Tu, S. M. Lukic, and I. Husain, "Hierarchical control for virtual oscillator based grid-connected and islanded microgrids," *IEEE Trans. Power Electron.*, vol. 35, no. 1, pp. 988–1001, Jan. 2020.

[4] Y. Han, H. Li, P. Shen, E. A. A. Coelho, and J. M. Guerrero, "Review of active and reactive power sharing strategies in hierarchical controlled microgrids," *IEEE Trans. Power Electron.*, vol. 32, no. 3, pp. 2427–2451, Mar. 2017.

[5] Y. Han, K. Zhang, H. Li, E. A. A. Coelho, and J. M. Guerrero, "MAS-based distributed coordinated control and optimization in microgrid and microgrid clusters: A comprehensive overview," *IEEE Trans. Power Electron.*, vol. 33, no. 8, pp. 6488–6508, Aug. 2018.

[6] A. J. Abianeh, Y. Wan, F. Ferdowsi, N. Mijatovic, and T. Dragicevic, "Vulnerability identification and remediation of FDI attacks in islanded DC microgrids using multiagent reinforcement learning," *IEEE Trans. Power Electron.*, vol. 37, no. 6, pp. 6359–6370, Jun. 2022.

[7] Y. Jiang, Y. Yang, S.-C. Tan, and S.-Y. R. Hui, "Distribution power loss mitigation of parallel-connected distributed energy resources in low-voltage DC microgrids using a Lagrange multiplier-based adaptive droop control," *IEEE Trans. Power Electron.*, vol. 36, no. 8, pp. 9105–9118, Aug. 2021.

[8] S. M. Malik, Y. Sun, W. Huang, X. Ai, and Z. Shuai, "A generalized droop strategy for interlinking converter in a standalone hybrid microgrid," *Appl. Energy*, vol. 226, pp. 1056–1063, Sep. 2018.

[9] S. Riverso, M. Tucci, J. C. Vasquez, J. M. Guerrero, and G. Ferrari-Trecate, "Stabilizing plug-and-play regulators and secondary coordinated control for AC islanded microgrids with bus-connected topology," *Appl. Energy*, vol. 210, pp. 914–924, Jan. 2018.

[10] A. Afshari, M. Karrari, H. R. Baghaee, G. B. Gharehpetian, and S. Karrari, "Cooperative fault-tolerant control of microgrids under switching communication topology," *IEEE Trans. Smart Grid*, vol. 11, no. 3, pp. 1866–1879, May 2020.

[11] A. Rafiee, Y. Batmani, F. Ahmadi, and H. Bevrani, "Robust load-frequency control in islanded microgrids: Virtual synchronous generator concept and quantitative feedback theory," *IEEE Trans. Power Syst.*, vol. 36, no. 6, pp. 5408–5416, Nov. 2021.

[12] J. Hu and P. Bhowmick, "A consensus-based robust secondary voltage and frequency control scheme for islanded microgrids," *Int. J. Elect. Power Energy Syst.*, vol. 116, Mar. 2020, Art. no. 105575.

[13] M. Raeispour, H. Atrianfar, H. R. Baghaee, and G. B. Gharehpetian, "Resilient h∞ consensus-based control of autonomous ac microgrids with uncertain time-delayed communications," *IEEE Trans. Smart Grid*, vol. 11, no. 5, pp. 3871–3884, Sep. 2020.

[14] K. Liu, P. Duan, Z. Duan, H. Cai, and J. Lu, "Leader-following consensus of multi-agent systems with switching networks and event-triggered control," *IEEE Trans. Circuits Syst. I, Reg. Papers*, vol. 65, no. 5, pp. 1696–1706, May 2018.

[15] M. Chen, X. Xiao, and J. M. Guerrero, "Secondary restoration control of islanded microgrids with a decentralized event-triggered strategy," *IEEE Trans. Ind. Inform.*, vol. 14, no. 9, pp. 3870–3880, Sep. 2018.

[16] J. Lai, X. Lu, X. Yu, and A. Monti, "Stochastic distributed secondary control for AC microgrids via event-triggered communication," *IEEE Trans. Smart Grid*, vol. 11, no. 4, pp. 2746–2759, Jul. 2020.
[17] Y. Wang, T. L. Nguyen, Y. Xu, Z. Li, Q.-T. Tran, and R. Caire, "Cyber-physical design and implementation of distributed event-triggered secondary control in islanded microgrids," *IEEE Trans. Ind. Appl.*, vol. 55, no. 6, pp. 5631–5642, Nov./Dec. 2019.
[18] J. Choi, S. I. Habibi, and A. Bidram, "Distributed finite-time event-triggered frequency and voltage control of AC microgrids," *IEEE Trans. Power Syst.*, vol. 37, no. 3, pp. 1979–1994, May 2022.
[19] Z. Chen, X. Yu, W. Xu, and G. Wen, "Modeling and control of islanded DC microgrid clusters with hierarchical event-triggered consensus algorithm," *IEEE Trans. Circuits Syst. I, Reg. Papers*, vol. 68, no. 1, pp. 376–386, Jan. 2021.
[20] F. Guo, L. Wang, C. Wen, D. Zhang, and Q. Xu, "Distributed voltage restoration and current sharing control in islanded DC microgrid systems without continuous communication," *IEEE Trans. Ind. Electron.*, vol. 67, no. 4, pp. 3043–3053, Apr. 2020.
[21] B. Fan, J. Peng, Q. Yang, and W. Liu, "Distributed periodic event-triggered algorithm for current sharing and voltage regulation in DC microgrids," *IEEE Trans. Smart Grid*, vol. 11, no. 1, pp. 577–589, Jan. 2020.
[22] J. Dai and G. Guo, "Event-triggered leader-following consensus for multi-agent systems with semi-Markov switching topologies," *Inf. Sci.*, vol. 459, pp. 290–301, Aug. 2018.
[23] Z. Zhang et al., "An event-triggered secondary control strategy with network delay in islanded microgrids," *IEEE Syst. J.*, vol. 13, no. 2, pp. 1851–1860, Jun. 2019.
[24] A. Fathi, Q. Shafiee, and H. Bevrani, "Robust frequency control of microgrids using an extended virtual synchronous generator," *IEEE Trans. Power Syst.*, vol. 33, no. 6, pp. 6289–6297, Nov. 2018.
[25] K. Jiang, H. Su, H. Lin, K. He, H. Zeng, and Y. Che, "A practical secondary frequency control strategy for virtual synchronous generator," *IEEE Trans. Smart Grid*, vol. 11, no. 3, pp. 2734–2736, May 2020.
[26] M. Ren, T. Li, K. Shi, P. Xu, and Y. Sun, "Coordinated control strategy of virtual synchronous generator based on adaptive moment of inertia and virtual impedance," *IEEE Trans. Emerg. Sel. Topics Circuits Syst.*, vol. 11, no. 1, pp. 99–110, Mar. 2021.
[27] X. Liang, C. Andalib-Bin-Karim, W. Li, M. Mitolo, and M. N. S. K. Shabbir, "Adaptive virtual impedance-based reactive power sharing in virtual synchronous generator controlled microgrids," *IEEE Trans. Ind. Appl.*, vol. 57, no. 1, pp. 46–60, Jan. 2021.
[28] M. Eskandari, L. Li, M. H. Moradi, P. Siano, and F. Blaabjerg, "Active power sharing and frequency restoration in an autonomous networked microgrid," *IEEE Trans. Power Syst.*, vol. 34, no. 6, pp. 4706–4717, Nov. 2019.
[29] L.-Y. Lu and C.-C. Chu, "Consensus-based droop control of isolated microgrids by ADMM implementations," *IEEE Trans. Smart Grid*, vol. 9, no. 5, pp. 5101–5112, Sep. 2018.
[30] M. Shi, X. Chen, J. Zhou, Y. Chen, and J. Wen, "Frequency restoration and oscillation damping of distributed VSGs in microgrid with low bandwidth communication," *IEEE Trans. Smart Grid*, vol. 12, no. 2, pp. 1011–1021, Mar. 2021.
[31] J. Liu, Y. Miura, and T. Ise, "Comparison of dynamic characteristics between virtual synchronous generator and droop control in inverter-based distributed generators," *IEEE Trans. Power Electron.*, vol. 31, no. 5, pp. 3600–3611, May 2016.
[32] X. Meng, J. Liu, and Z. Liu, "A generalized droop control for grid-supporting inverter based on comparison between traditional droop control and virtual synchronous generator control," *IEEE Trans. Power Electron.*, vol. 34, no. 6, pp. 5416–5438, Jun. 2019.
[33] W. Ren and R. Beard, "Consensus seeking in multiagent systems under dynamically changing interaction topologies," *IEEE Trans. Autom. Control*, vol. 50, no. 5, pp. 655–661, May 2005.
[34] J. Hu and Y. Hong, "Leader-following coordination of multi-agent systems with coupling time delays," *Physica A, Statist. Mechanics Appl.*, vol. 374, no. 2, pp. 853–863, Feb. 2007.
[35] L. Zhu, Z. Chen, and R. H. Middleton, "A general framework for robust output synchronization of heterogeneous nonlinear networked systems," *IEEE Trans. Autom. Control*, vol. 61, no. 8, pp. 2092–2107, Aug. 2016.
[36] N. Pogaku, M. Prodanovic, and T. C. Green, "Modeling, analysis and testing of autonomous operation of an inverter-based microgrid," *IEEE Trans. Power Electron.*, vol. 22, no. 2, pp. 613–625, Mar. 2007.
[37] C. Ahumada, R. Cardenas, D. Saez, and J. M. Guerrero, "Secondary control strategies for frequency restoration in islanded microgrids with consideration of communication delays," *IEEE Trans. Smart Grid*, vol. 7, no. 3, pp. 1430–1441, May 2016.
[38] A. Bidram, A. Davoudi, F. L. Lewis, and J. M. Guerrero, "Distributed cooperative secondary control of microgrids using feedback linearization," *IEEE Trans. Power Syst.*, vol. 28, no. 3, pp. 3462–3470, Aug. 2013.
[39] F. Guo, C. Wen, J. Mao, and Y.-D. Song, "Distributed secondary voltage and frequency restoration control of droop-controlled inverter-based microgrids," *IEEE Trans. Ind. Electron.*, vol. 62, no. 7, pp. 4355–4364, Jul. 2015.
[40] J. W. Simpson-Porco, Q. Shafiee, F. Dorfler, J. C. Vasquez, J. M. Guerrero, and F. Bullo, "Secondary frequency and voltage control of islanded microgrids via distributed averaging," *IEEE Trans. Ind. Electron.*, vol. 62, no. 11, pp. 7025–7038, Nov. 2015.

Jiancheng Zhang received the B.S. degree in mechanical engineering and automation from Huabei Polytechnic University, Tangshan, China, in 2010, the M.S. degree in mechanical and electronic engineering from Harbin Institute of Technology, Shenzhen, China, in 2013, and the Ph.D. degree in control science and engineering from Harbin Institute of Technology, Harbin, China, in 2022.

From 2014 to 2018, he worked in the 513 Research Institute of China Aerospace Fifth Research Institute, JIER Machine Tool Group Co., Ltd. and Oriental Bluesky Titanium Technology Company, Ltd., where he served as an Engineer and was responsible for product R&D. He is now a postdoctoral fellow of control science and engineering in Shandong University, Jinan, China. His research interests include multiagent cooperative control, artificial intelligence, and their application in microgrid.

Bo Sun (Member, IEEE) received the B.S. and Ph.D. degrees in control theory and control engineering from Shandong University, Jinan, China, in 2004 and 2009, respectively.

He joined Shandong University, in 2010, where he is currently a Professor with the School of Control Science and Engineering. His current research interests include optimal control of engineering and combined cooling, heating, and power system.

Daduan Zhao (Member, IEEE) received the B.S. degree in electronic information science and technology from Qufu Normal University, Rizhao, China, in 2015 and the M.S. degree in signal and information processing from Southwest University, Chongqing, China, in 2018. He is currently working toward the Ph.D. degree in control theory and control engineering with Shandong University, Jinan, China.

His current research interests include multiagent systems, distributed optimization, and ac/dc microgrids.